

Figure 4.6b Type 4 isotherm compared to an activated alumina isotherm [120] and type 5 isotherm compared to a charcoal isotherm [117]

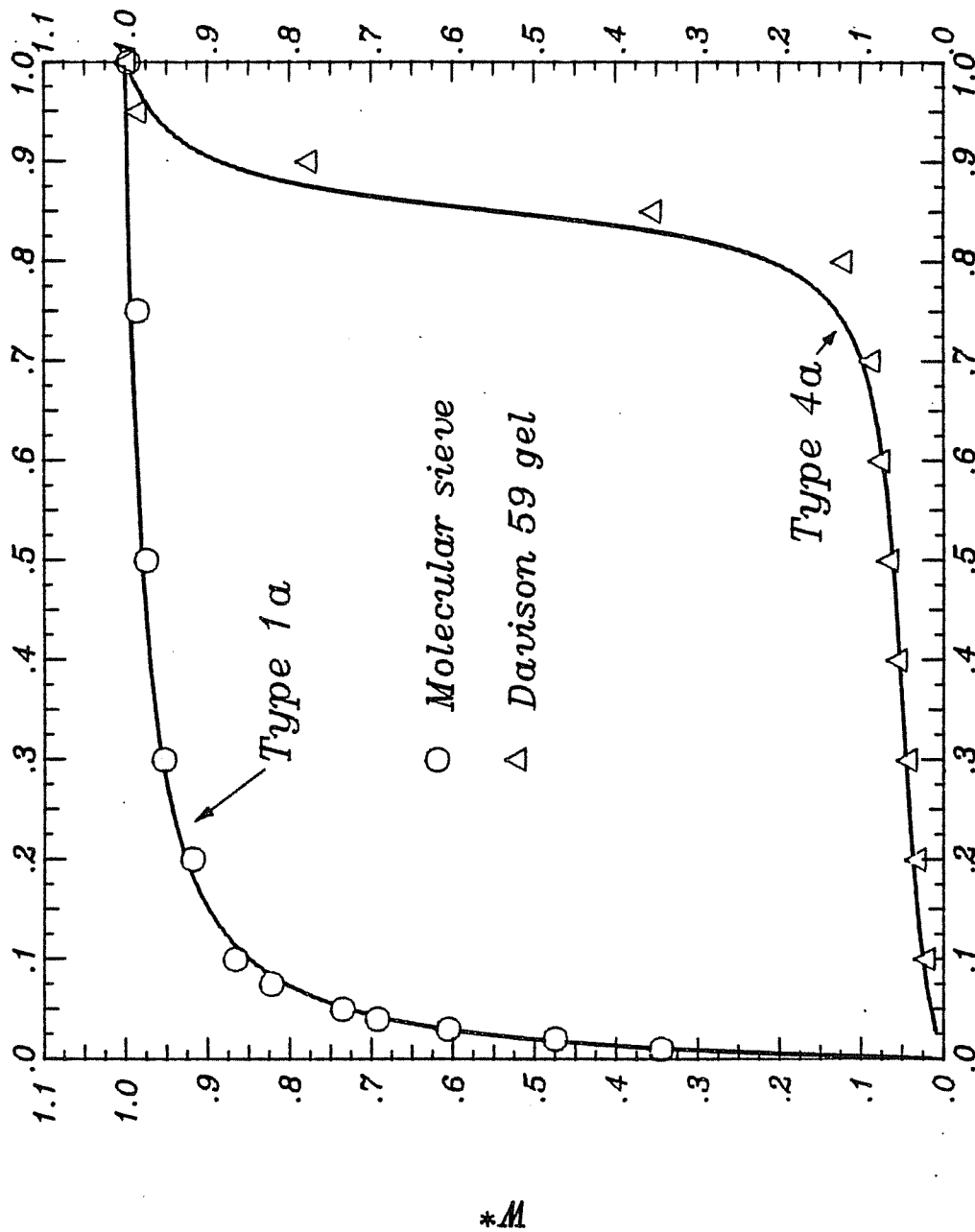


Figure 4.6c Types 1a and 4a isotherms compared to isotherms for molecular sieve and macroporous silica gel [110]

R

Thus,

$$h^*(W^*) = 1 + h^* \frac{\exp(kW^*) - \exp(k)}{1 - \exp(k)} \quad (4.8)$$

The advantage of the form of $h^*(W^*)$ given by Eq. (4.8) over that of Eq. (4.7) is that since $h^*(W^* = 1.0) = 1.0$, from Eq. (4.3) it can be deduced that at $r = 1$, $W = W_{mx}$ regardless of temperature. Since the isotherms converge to W_{mx} at $r = 1$, W_{mx} is a convenient scaling parameter. The physical assumption implicit in the variation of h^* given by Eq. (4.8) is that at $r = 1$ (saturated air), adsorption becomes normal condensation on the matrix.

The constants Δh^* and k for Eq. (4.8) were selected primarily on the basis on Brandemuehl's analysis of silica gel data. The nominal values of Δh^* and k are 0.3 and -5.0 for the types 1,2,4 and linear isotherms. For the type 3 and type 5 isotherms, $\Delta h^* = -0.3$ since the heat of sorption is less than the heat of water vaporization for these adsorbents (§4.2). The type 5 isotherm required $k = -7.5$ to prevent the isotherm from being double valued at low temperatures. In all cases considered in this study the parameter t_0 (Eq. (4.3)), the temperature at which $r = G(W^*)$, is 60°C. An example of the typical variation of the isotherms with temperature is shown in Figure 4.7, where the type 1 isotherm is illustrated.

To determine the effect of the heat of adsorption on dehumidifier performance, h^* was varied for the linear isotherm. In addition to the nominal parameters, both $\Delta h^* = 0$ and $\Delta h^* = 1.0$, $k = 1.0$

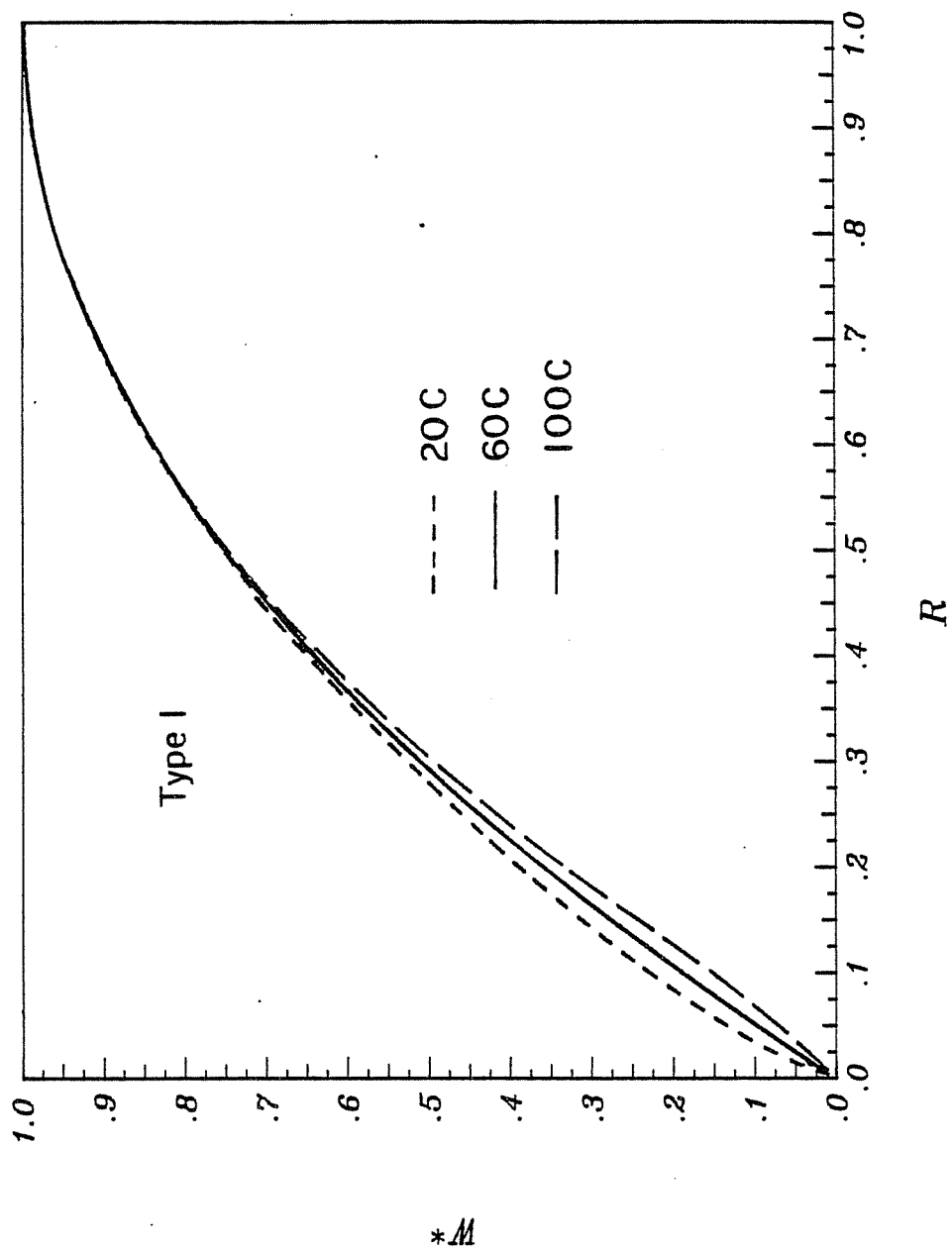


Figure 4.7 Temperature variation of the type 1 isotherm

were used. The effect of these perturbations on the temperature response of the linear isotherm is shown in Figure 4.8.

4.3.3 Maximum Water Content

The form selected for $h^*(W)$, Eq. (4.8), insures that the water content of the adsorbent at saturation is independent of temperature. The maximum water content of the adsorbent, W_{mx} , can be used as a scaling parameter. A survey of the isotherms discussed in §4.2.2 and §4.3.1 shows that W_{mx} varies considerably. The microporous silica gels, activated aluminas and charcoals have W_{mx} in the range of 0.35 to 0.5 (g water)/(g dry adsorbent). Molecular sieves have W_{mx} in the range of 0.2 to 0.3 g/g. At the other extreme, W_{mx} for the macroporous silica gels can be greater than 1.0 g/g.

A nominal value of $W_{mx} = 0.5$ is used to determine the effect of isotherm shape on dehumidifier performance (§4.4.1). This comparison is based on types 1-5 and the linear isotherm (Eqs. (4.6.1) - (4.6.6)). The linear isotherm is used to indicate the effect on dehumidifier performance of varying W_{mx} to 0.25 g/g and 1.0 g/g. In order to better model actual adsorbents, and to gauge the combined effect of isotherm shape and W_{mx} on dehumidifier performance, the type 1a isotherm with $W_{mx} = 0.25$ (molecular sieve) and the type 4a isotherm with $W_{mx} = 1.125$ (macroporous silica gel) were also simulated. These comparisons will allow the effects of isotherm shape, W_{mx} , and material type to be considered independently.

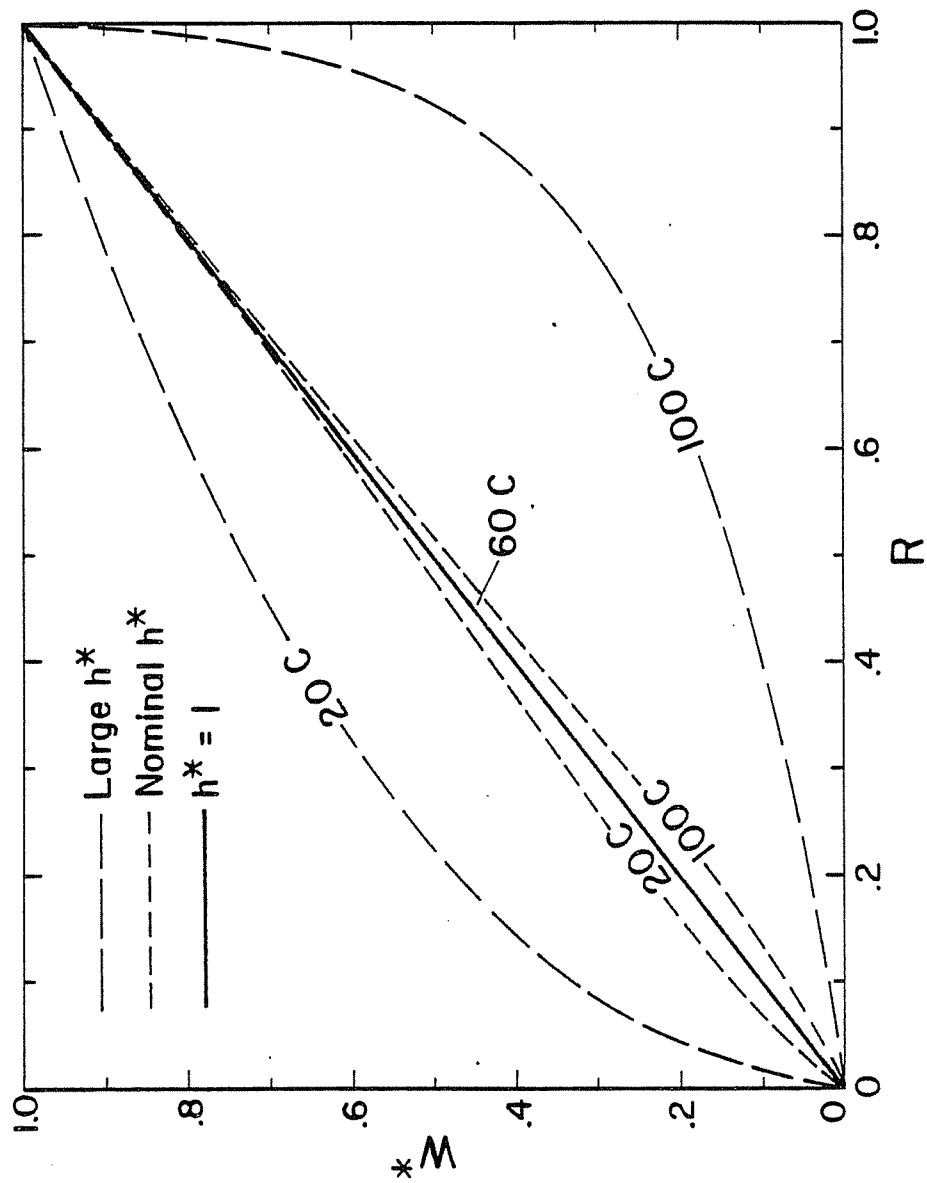


Figure 4.8 Variation of the linear isotherm with temperature for three different variations of the heat of adsorption

4.3.4 Adsorption Hysteresis

An example of a hysteresis loop in an adsorbent is illustrated by the sorption-desorption isotherm for Davison 03 silica gel [119] illustrated in Figure 4.9. The effect of hysteresis in a microporous adsorbent was modeled by using the linear isotherm in the adsorbing (process) period of the dehumidifier, and the type 1 isotherm in the desorbing (regenerating) period. Since the Clausius-Clapeyron relation (Eq. (4.1)) can not apply in this situation, $\Delta h^*=0$ was used for both branches of the hysteresis isotherm. This results in the hysteresis loop being independent of temperature.

Modeling the sorption hysteresis isotherm by a simple superposition of two isotherms does not allow intermediate paths to be followed between the sorption and desorption branches of the isotherm, as is often observed [118]. However, this model provides an upper bound estimate of the effect of adsorption hysteresis on dehumidifier performance.

4.3.5 Matrix Moisture Diffusivity

A major assumption required to develop the dehumidifier model (§2.4) is that the combined process of diffusion in the matrix and convection at the matrix surface can be described by composite or lumped transfer coefficients. The ratio of overall heat transfer coefficient to the product of overall mass transfer coefficient and moist air thermal capacitance is called the overall Lewis number,

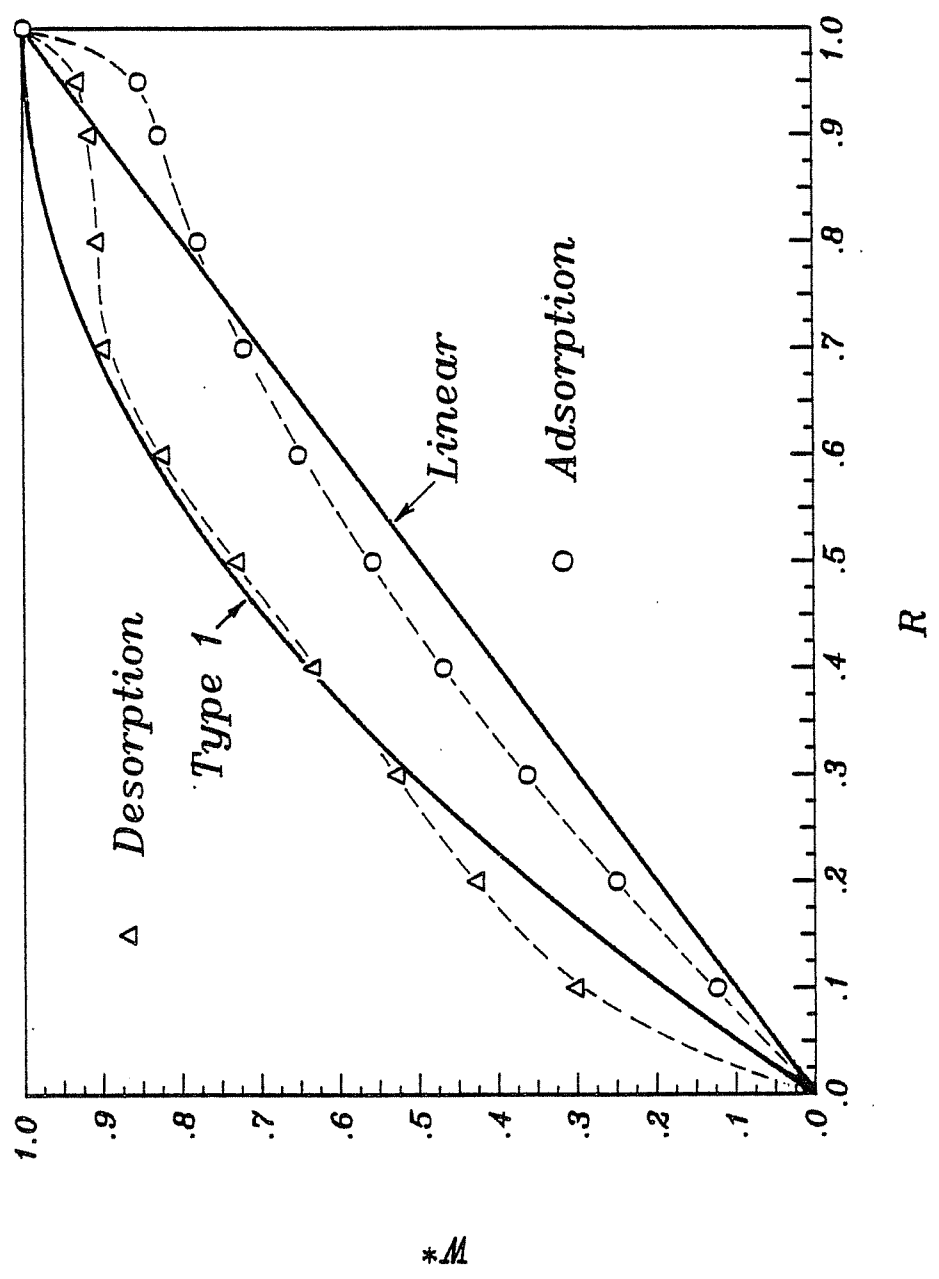


Figure 4.9 Adsorption-desorption isotherm hysteresis for Davison 03 silica gel [119]

Le_o . If the resistances to diffusion into the matrix in a direction normal to the air flow are small, the overall transfer coefficients are governed by the convective film resistances. For the air-water vapor system, the convective Lewis number is near unity. Banks [35] has estimated that Le_o is at least 2.0 for parallel passage dehumidifiers, and van Leersum's results [37] indicate that $Le_o = 4.0$ is a lower limit for packed bed dehumidifiers. A nominal value of $Le_o = 1.0$ is employed in this study. The linear isotherm with $Le_o = 4.0$ is used to indicate the effect of matrix diffusional resistance on dehumidifier performance.

4.3.6 Matrix Thermal Capacitance

Two common matrix configurations were described in 2.1, the parallel passage wheel and the packed bed. In either configuration, a certain amount of non-adsorbing material is used in the matrix. The proportion of inert to adsorbent material in a parallel passage matrix can be considerably greater than in a packed bed, since the desiccant must be deposited on a substrate film rather than be used in bulk form.

The nominal value of matrix thermal capacitance used in this study is $921 \text{ J}/(\text{kg}\text{-}^\circ\text{C})$, the bulk thermal capacitance of silica gel [110], so that the contribution of the inert matrix materials to the thermal capacitance is neglected. To test the extreme effect of matrix thermal capacity on dehumidifier performance, the linear isotherm with $c_m = 3350 \text{ J}/(\text{kg}\text{-}^\circ\text{C})$ was studied. This value of c_m

corresponds to a desiccant-substrate system which is either 50% mylar or 44% aluminum foil by volume and is an upper limit for conventional dehumidifier designs [56].

4.3.7 Flow Parameters

A balanced air mass of low rate and symmetric flow area counterflow dehumidifier is modeled in the parametric study. The nominal value of the overall number of transfer units for mass transfer, NTU_w , is 10, which is representative of high performance dehumidifiers. A range of rotational speeds is considered. The parameter μ_k is varied from 0.05 to 5.0, resulting in both dehumidifier and enthalpy regenerator operation. The regenerator performance is determined for two pairs of air inlet states: Inlet state pair 1 ((35°C, 14.2 g/kg), (85°C, 14.2 g/kg)) from §3.5 is again employed. The process and regenerating stream inlet relative humidities for this pair are 40% and 4%. The second inlet state pair used in §3.5 had inlet relative humidities at 50% and ~5%. Because this choice would have resulted in a very narrow range of inlet relative humidities in the parametric study, an alternative inlet state pair of ((30°C, 24.5 g/kg), (100°C, 14.2 g/kg)) with inlet relative humidities of 91% and 2% is substituted. The inlet state pairs used in §4.4 are referred to as 1 and 2, but the reader is again cautioned that the inlet state pair 2 employed in §4.4 is not the same as the one used in §3.5.

4.4 Dehumidifier Performance: Results and Discussion

The main function of the dehumidifier is to reduce the process stream humidity ratio. While in desiccant air conditioning systems the process stream outlet temperature affects system performance (§4.5), in this discussion the process outlet humidity ratio will be of primary interest. The dehumidifier performance is characterized by a dehumidifier efficiency, η_w , determined as

$$\eta_w = \frac{w_{1,2} - w_{1,1}}{w_{a,int} - w_{1,1}} \quad (4.9)$$

where $w_{1,2}$ and $w_{1,1}$ are the process stream outlet and inlet humidity ratios, and $w_{a,int}$ is the humidity ratio at the intersection point of the line of constant adiabatic saturation temperature through the process inlet state and a relative humidity line through the regenerating inlet state, as shown in Figure 4.10. The minimum potential humidity ratio would be $w_{a,int}$ if the dehumidification process were the reverse of an adiabatic saturation process with air exiting the dehumidifier at the relative humidity of the regenerating state. In fact, the dehumidification potential lines depend on the matrix properties as well as the moist air properties, and are skewed away from wet bulb and relative humidity lines (§3.1), so $w_{a,int}$ is only a convenient normalizing parameter.

The dehumidifier outlet states are influenced by μK , the ratio of matrix rotational mass flow rate to air mass flow. For example,

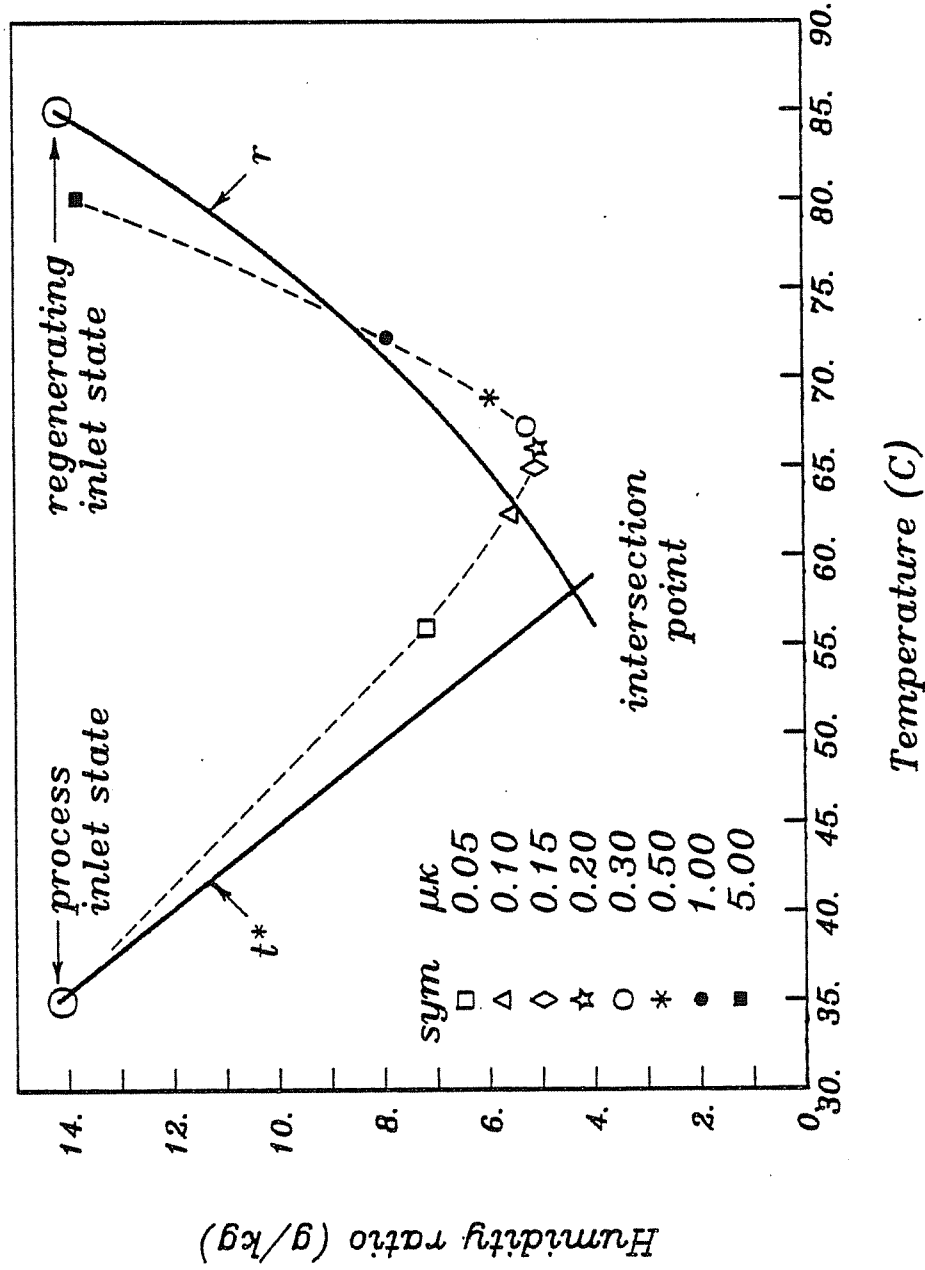


Figure 4.10 Variation of the dehumidifier process stream outlet states with $\mu\kappa$, superimposed on a wet bulb temperature (t^*) line through the process stream inlet state and a relative humidity (r) line through the regenerating stream inlet state

the variation of dehumidifier outlet states with μ_K is shown in Figure 4.10 for the nominal linear isotherm. The optimum μ_K for dehumidification, μ_{K_x} , varies with dehumidifier inlet states and matrix properties. In much of the discussion that follows, only the results for μ_{K_x} will be given, along with an indication of the sensitivity of η_w to μ_K .

4.4.1 Isotherm Shape

Table 4.6 gives μ_{K_x} , $t_{1,2}$ and $w_{1,2}$, and η_{wx} for the types 1-5 and the linear isotherms. The results show that the isotherms can easily be classified in two groups, one favorable and the other unfavorable for dehumidification.

The types 1, 2, and 4 and linear isotherms have relatively high η_{wx} , and can be considered favorable for dehumidification. The type 1 isotherm has the highest η_{wx} for both inlet states, at 0.96 for inlet state 1 and 0.91 for inlet state 2. The types 2, 4 and linear isotherms all have approximately the same performance for inlet state 1, with $\eta_{wx} \approx 0.93$. For inlet state 2, the type 2 and linear isotherms have $\eta_{wx} \approx 0.86$, while the type 4 isotherm has $\eta_{wx} \approx 0.88$. Thus, the type 1 isotherm results in η_{wx} about 5% greater than for the other favorable isotherms. The favorable isotherm η_{wx} for inlet state pair 1 are about 5-7% greater than the η_{wx} for inlet state pair 2.

The types 3 and 5 isotherms have η_{wx} substantially lower than for the first group, and can be considered unfavorable for de-

humidification. For inlet state 1, the η_{wx} for the type 3 isotherm is 0.77 and for the type 5 isotherm η_{wx} is 0.75, some 20% less than the mean η_{wx} for the favorable isotherms. Both of the unfavorable isotherms have η_{wx} for inlet state 2 that are slightly greater than for inlet state 1.

The results in Table 4.6 also indicate that the optimum rotational speed varies with matrix properties and dehumidifier inlet states. The favorable isotherms have a much lower $\mu\kappa_x$ than the unfavorable isotherms, corresponding to a lower optimum matrix rotational speed at a given air flow rate. However, $\mu\kappa_x$ varies more with the change in inlet state for the favorable isotherms than for the unfavorable types. For any of the favorable isotherms, $\mu\kappa_x$ for inlet state 2 is about twice $\mu\kappa_x$ for inlet state 1, representing a doubling in optimum matrix rotational speed as the inlet states change. The changes in $\mu\kappa_x$ for the unfavorable isotherms are proportionally smaller than the changes in $\mu\kappa_x$ with inlet state for the favorable isotherms.

To indicate the effect of operating the dehumidifier at non-optimum rotational speeds, Table 4.7 lists the values of $t_{1,2}$, $w_{1,2}$ and η_w at $\mu\kappa$ equal to $\mu\kappa_x$ for the alternate inlet state pair. Comparing the results given in Tables 4.6 and 4.7, it can be seen that operating at the non-optimal $\mu\kappa$ results in an average drop in η_w of about 4% from η_{wx} . This implies that near optimum dehumidification is obtained over a reasonably broad range of $\mu\kappa$. In practice, if modulating $\mu\kappa$ in response to changes in inlet state is not

Table 4.6 Effect of Isotherm Shape on Optimum Dehumidifier Performance

Type	Inlet State 1				Inlet State 2			
	μ_K	$t_{1,2} (^{\circ}\text{C})$	$w_{1,2} (\frac{\text{g}}{\text{kg}})$	η_{wx}	μ_K	$t_{1,2} (^{\circ}\text{C})$	$w_{1,2} (\frac{\text{g}}{\text{kg}})$	η_{wx}
1	0.12	63.84	4.729	0.965	0.22	82.03	6.918	0.911
2	0.17	65.65	5.154	0.922	0.30	84.09	7.879	0.862
3	0.50	66.36	6.678	0.766	0.60	82.35	9.080	0.799
4	0.17	65.58	5.124	0.925	0.28	83.80	7.620	0.875
5	0.55	67.63	7.096	0.727	0.70	83.88	10.252	0.739
linear	0.18	65.64	5.081	0.929	0.35	84.02	7.914	0.860

Table 4.7 Dehumidifier Performance at μ_K Away From the Optimum

Type	Inlet State 1				Inlet State 2			
	μ_K	$t_{1,2} (^{\circ}\text{C})$	$w_{1,2} (\frac{\text{g}}{\text{kg}})$	η_w	μ_K	$t_{1,2} (^{\circ}\text{C})$	$w_{1,2} (\frac{\text{g}}{\text{kg}})$	η_w
1	0.22	65.26	5.053	0.932	0.12	79.04	7.299	0.892
2	0.30	67.34	5.441	0.892	0.17	80.67	8.380	0.836
3	0.60	67.99	6.904	0.743	0.50	79.97	9.229	0.792
4	0.28	66.99	5.408	0.896	0.17	81.17	7.968	0.857
5	0.70	69.85	7.341	0.699	0.55	79.86	10.498	0.726
linear	0.35	67.65	5.467	0.890	0.18	79.85	8.413	0.834

feasible, a mean value of μK will result in satisfactory performance.

Except for the clear distinction between the high performance favorable isotherms and the low performance unfavorable isotherms, the variations in isotherm type, μK , and inlet state result in at most 5-7% variations in η_w . This suggests that provided a favorable isotherm is selected (noting the assumption that all other parameters are equal), the performance of the dehumidifier is not sensitive to isotherm shape or operating condition. However, measuring these effects as proportional changes in η_w masks the fact that the changes in high performance dehumidifier design required to offset a 5% variation in η_w with matrix properties can be large. For example, Table 4.8 lists the NTU_o required at μK_x for the various isotherms to have $\eta_w = 0.95$ for inlet state 1 and $\eta_w = 0.90$ for inlet state 2. The results show that the NTU_o required for a given η_w by the type 2,4 and linear isotherm dehumidifiers is about twice that of a type 1 isotherm dehumidifier. The type 3 and 5 isotherm dehumidifiers can not obtain the required η_w at NTU_o more than four times the type 1 dehumidifier. Thus, other variables being equal, the volume of the type 1 dehumidifier will be at most half that of the alternative designs. The seemingly insignificant performance advantage of the type 1 isotherm dehumidifier is magnified when viewed in this perspective.

Table 4.8 NTU_o required to obtain $\eta_{wx} = 0.95$ for inlet state 1
 $\eta_{wx} = 0.90$ for inlet state 2

Type	Inlet State 1			Inlet State 2		
	μK_x	NTU_o	η_w	μK_x	NTU_o	η_w
1	0.12	8.0	0.950	0.22	8.5	0.899
2	0.17	19.0	0.951	0.30	20.0	0.899
3	0.50	40.0	0.841	0.60	40.0	0.865
4	0.17	17.5	0.949	0.28	15.0	0.900
5	0.50	40.0	0.801	0.75	40.0	0.792
linear	0.18	15.0	0.951	0.35	20.0	0.899

4.4.2 Heat of Adsorption

Table 4.9 illustrates the effect of the heat of adsorption on the optimum dehumidifier performance for an isotherm that is linear at 60°C. The data shown are for the temperature independent ($\Delta h^* = 0.0$) isotherm, the nominal isotherm ($\Delta h^* = 0.3$), and the strongly temperature dependent isotherm ($\Delta h^* = 1.0$, $k = -1.0$) illustrated in Figure 4.8.

The results show a pronounced effect on dehumidifier performance of a large increase in the heat of adsorption. The strongly temperature dependent isotherm ($\Delta h^* = 1.0$) has η_{wx} about 10% less than the other linear isotherms for inlet state 1, and about 25% less for inlet state 2. The data from which Table 4.9 was abstracted show that for μk between 0.10 and 0.50 the process outlet temperatures for the strongly temperature dependent isotherm dehumidifier vary from 10°C to 6°C higher than the outlet temperatures at the same μk for the temperature independent isotherm. The strongly temperature dependent isotherm thus results in substantially hotter and wetter dehumidifier process outlet states than are obtained with the temperature independent isotherm. This is a result of the large amount of additional energy liberated on adsorption, which tends to increase the matrix and air temperatures and has an adverse effect on the absorptive capacity of the matrix.

The comparison between the nominal linear isotherm and the temperature independent isotherm is somewhat more ambiguous. The

Table 4.9 Effect of heat of adsorption on optimum dehumidifier performance

Δh^*	Inlet State 1			Inlet State 2				
	μ_{K_x}	$t_{1,2} (^{\circ}\text{C})$	$w_{1,2} (\frac{\text{g}}{\text{kg}})$	η_{wx}	μ_{K_x}	$t_{1,2} (^{\circ}\text{C})$	$w_{1,2} (\frac{\text{g}}{\text{kg}})$	η_{wx}
0.0	0.18	62.53	5.188	0.918	0.30	80.58	7.229	0.895
0.3	0.18	65.64	5.081	0.929	0.35	84.02	7.914	0.860
1.0	0.20	72.14	6.217	0.813	0.50	89.44	11.306	0.684

outlet temperatures for the nominal isotherm are roughly 3°C higher than those for the temperature independent isotherm for $\mu\kappa$ between 0.10 and 0.50, which is consistent with results obtained for the strongly temperature dependent isotherm. However, for inlet state 1, the process outlet humidity ratios for the nominal isotherm are slightly less than those for the temperature independent isotherm in the 0.10 to 0.50 $\mu\kappa$ range, while for inlet state 2, the nominal isotherm has outlet humidity ratios that are greater than those for the temperature independent isotherm.

These results indicate that while small heat effects associated with adsorption may be beneficial, large heats of adsorption, which result in strongly temperature dependent isotherms, have an adverse effect on the performance of the dehumidifier.

4.4.3 Maximum Water Content

The maximum water content, W_{mx} , for the linear isotherm was varied from its nominal value of 0.50 to 0.25 and 1.0. The effect of this variation on the optimum dehumidifier performance is shown in Table 4.10.

The data in Table 4.10 show that as W_{mx} increases, $\mu\kappa_x$ decreases while η_{wx} increases. For inlet state 1, η_{wx} increases by about 9%, from 0.88 to 0.96, as W_{mx} is increased from 0.25 to 1.0. The corresponding increase in η_{wx} for inlet state 2 is about 11%, from 0.80 to 0.90.

Table 4.10 Effects of W_{mx} on optimum dehumidifier performance

W_{mx}	Inlet State 1				Inlet State 2			
	μ_{K_x}	$t_{1,2} (^{\circ}\text{C})$	$w_{1,2} (\frac{\text{g}}{\text{kg}})$	η_{wx}	μ_{K_x}	$t_{1,2} (^{\circ}\text{C})$	$w_{1,2} (\frac{\text{g}}{\text{kg}})$	η_{wx}
0.25	0.30	67.69	5.591	0.877	0.50	85.55	9.044	0.801
0.50	0.18	65.64	5.081	0.929	0.35	84.02	7.914	0.860
1.00	0.10	64.20	4.792	0.958	0.22	82.67	7.180	0.898

Although increasing W_{mx} is beneficial to dehumidifier performance, the η_{wx} for the type 1 isotherm with $W_{mx} = 0.50$ (Table 4.6) are greater than the η_{wx} for the linear isotherm with $W_{mx} = 1.0$. Changing the isotherm shape from linear to type 1 at $W_{mx} = 0.50$ has a greater beneficial effect on η_{wx} than increasing W_{mx} of the linear isotherm from 0.50 to 1.0. Also, since the η_{wx} for the $W_{mx} = 1.0$ linear isotherm are approximately 0.95 and 0.90, from the results in Table 4.8, it can be deduced that the nominal linear isotherm would require the dehumidifier NTU_o to be twice that of the NTU_o of the $W_{mx} = 1.0$ isotherm dehumidifier to achieve the same performance. It was determined that the $W_{mx} = 0.25$ isotherm requires the dehumidifier NTU_o to be increased to more than 40 to obtain the η_{wx} of the $W_{mx} = 1.0$ isotherm dehumidifier with $NTU_o = 10$.

Since perturbation in the isotherm shape can have as much effect on dehumidifier performance as doubling W_{mx} , the combined effect of isotherm shape and W_{mx} was considered by modeling three generic desiccants. Isotherm type 1a with $W_{mx} = 0.25$, type 1 with $W_{mx} = 0.50$, and type 4a with $W_{mx} = 1.125$ were used to represent molecular sieves, microporous adsorbents, and macroporous adsorbents. The η_{wx} shown in Table 4.11 indicate that the microporous adsorbent with the type 1 isotherm has by far the superior performance. The macroporous adsorbent performs slightly better than the molecular sieve, though W_{mx} for the macroporous desiccant is over four times that of the molecular sieve.

Table 4.11 Comparison of molecular sieve, micro porous gel, and macroporous gel dehumidifier performance

Desiccant Type	Inlet State 1				Inlet State 2			
	μK_x	$t_{1,2} (^{\circ}C)$	$w_{1,2} (\frac{g}{kg})$	η_{WX}	μK_x	$t_{1,2} (^{\circ}C)$	$w_{1,2} (\frac{g}{kg})$	η_{WX}
Mole Sieve	0.15	64.46	6.153	0.820	0.30	84.89	9.694	0.767
Micro Gel	0.12	63.84	4.729	0.965	0.22	82.03	6.918	0.911
Macro G	0.30	62.82	6.028	0.832	0.50	84.97	8.814	0.813

4.4.4 Adsorption Hysterisis

The performance of a dehumidifier with a linear adsorption--type 1 desorption hysterisis isotherm is compared with that of a reversible linear isotherm in Table 4.12 for values of $\mu\kappa$ that scan the optimum range for the reversible linear isotherm. The desorption hysterisis loop has a very pronounced adverse effect on the performance of the dehumidifier. The η_w for the hysterisis isotherm shown in Table 4.12 are between 15% and 30% less than the η_w for the reversible linear isotherm. This corresponds to a decrease in the apparent NTU_o of the dehumidifier from 10 to about 2.5, i.e., a linear isotherm dehumidifier with $NTU_o = 2.5$ ($Le_o = 1$) has roughly the same η_w as the hysterisis isotherm dehumidifier with $NTU_o = 10$.

4.4.5 Matrix Moisture Diffusivity

The results in the preceeding sections have been for dehumidifiers in which the transfer processes are controlled by the convective film resistances ($Le_o = 1$). The data in Table 4.13 show the effect on the performance of a linear isotherm dehumidifier of increasing Le_o from 1.0 to 4.0 at constant $NTU_t = 10$, corresponding to an increase in the matrix resistance to water vapor diffusion. Increasing Le_o to 4.0 decreases η_{wx} by about 8%. This performance can be obtained by an $Le_o = 1$ exchanger with $NTU_o \approx 4.5$. Decreasing NTU_w by a factor of 4 at constant NTU_t has the same

Table 4.12 Effect of isotherm hysteresis on dehumidifier performance

Isotherms Proc/Reg	Inlet State 1				Inlet State 2			
	μK	$t_{1,2} (^{\circ}\text{C})$	$w_{1,2} (\frac{\text{g}}{\text{kg}})$	η_w	μK	$t_{1,2} (^{\circ}\text{C})$	$w_{1,2} (\frac{\text{g}}{\text{kg}})$	η_w
lin/lin	0.10	58.89	5.793	0.857	0.20	77.58	7.616	0.875
lin/lin	0.15	61.605	5.260	0.911	0.25	79.39	7.320	0.891
lin/lin	0.20	62.99	5.196	0.917	0.30	80.58	7.229	0.895
lin/l	0.10	55.28	7.457	0.687	0.20	72.74	9.832	0.760
lin/l	0.15	56.70	7.557	0.677	0.25	73.78	10.011	0.751
lin/l	0.20	57.57	7.872	0.645	0.30	74.56	10.285	0.737

Table 4.13 Effect of Le_o on dehumidifier performance

NTU/Le _t _o	Inlet State 1				Inlet State 2			
	μK_x	$t_{1,2} (^{\circ}\text{C})$	$w_{1,2} (\frac{\text{g}}{\text{kg}})$	η_{wx}	μK_x	$t_{1,2} (^{\circ}\text{C})$	$w_{1,2} (\frac{\text{g}}{\text{kg}})$	η_{wx}
10/1	0.18	65.64	5.081	0.929	0.35	84.02	7.914	0.860
10/4.0	0.17	63.64	5.836	0.852	0.28	80.34	9.193	0.793

effect of halving NTU_o at $LE_o = 1$. The volume of the $LE_o = 4$ dehumidifier is therefore about twice that of an $LE_o = 1$ dehumidifier with the same performance.

Since an increase in LE_o at fixed NTU_t is equivalent to an increase in mass transfer resistance in the matrix, another way to interpret the effect of the hysteresis isotherm (§4.4.4) on dehumidifier performance is to determine the apparent LE_o of an $NTU_t = 10$ exchanger that results in the same performance as obtained using the hysteresis isotherm. As shown by the data in Table 4.14, the effect of the hysteresis isotherm is equivalent to LE_o ranging from 9.0 to 13.0. Both the outlet temperatures and humidity ratios of the hysteresis isotherm dehumidifier can be closely matched using a single value of LE_o . This implies that if estimates of LE_o are to be empirically obtained by matching predictions of a convective transfer dehumidifier model with experimental data for the dehumidifier outlet states, care must be exercised to avoid confusing the effects of matrix diffusion resistance and adsorption hysteresis.

4.4.6 Matrix Thermal Capacitance

The previous results were based upon a matrix thermal capacitance corresponding to the bulk thermal capacitance of silica gel. The results in Table 4.15 show the effect of increasing c_m from 921 (J/(kg-°C)) to 3350 (J/(kg-°C)), corresponding to a matrix composition that is 50% mylar by volume. The increase in c_m results in about a 15% decrease in η_{wx} and a reduction in the

Table 4.14 Le_o required to match the linear isotherm and hysteresis isotherm dehumidifier performance for inlet state 1

Hysteresis Isotherm			Linear Isotherm					
$\mu\kappa$	$t_{1,2} (^{\circ}\text{C})$	$w_{1,2} (\frac{\text{g}}{\text{kg}})$	η_x	Le_o	$\mu\kappa$	$t_{1,2} (^{\circ}\text{C})$	$w_{1,2} (\frac{\text{g}}{\text{kg}})$	η_w
0.10	53.28	7.457	0.687	9.25	0.10	55.04	7.441	0.689
0.15	56.70	7.557	0.677	11.50	0.15	56.51	7.547	0.678
0.20	57.57	7.872	0.645	13.00	0.30	57.48	7.863	0.646

Table 4.15 Effect of matrix thermal capacitance on dehumidifier performance

C_m ($\frac{\text{J}}{\text{kg}\cdot^{\circ}\text{C}}$)	Inlet State 1			Inlet State 2				
	$\mu\kappa_x$	$t_{1,2} (^{\circ}\text{C})$	$w_{1,2} (\frac{\text{g}}{\text{kg}})$	η_{wx}	$\mu\kappa_x$	$t_{1,2} (^{\circ}\text{C})$	$w_{1,2} (\frac{\text{g}}{\text{kg}})$	η_{wx}
921	0.18	65.64	5.081	0.929	0.35	84.02	7.914	0.860
3350	0.115	69.60	6.285	0.806	0.17	86.77	10.409	0.730

values of μK_x . The results for μK between 0.10 and 0.50 show that at a given μK , the process stream outlet temperatures for the large c_m dehumidifier are between 5°C and 7°C higher than those for the nominal case, while the outlet humidity ratios are substantially greater. Increasing c_m results in significantly hotter and wetter process stream outlet states.

Comparing the results for $c_m = 3550$ (J/(kg-°C)) in Table 4.15 with those for $\Delta h^* = 1$ in Table 4.9, it can be seen that the increased sensible heat effects associated with large c_m cause roughly the same decrease in η_{wx} as the large latent heat effects associated with large Δh^* . Similarly, comparison of the results for large c_m in Table 4.15 with those for $W_{mx} = 0.25$ in Table 4.10 and for $Le_o = 4$ in Table 4.13 shows that increasing c_m has a larger adverse effect on η_{wx} than does decreasing W_{mx} or increasing Le_o .

The results of §4.4.2 for large heat of adsorption and this section for large c_m indicate that large latent or sensible heat effects have a significant detrimental impact on the performance of the dehumidifier.

4.5 Desiccant Cooling System Performance: Results and Discussion

In §4.4, the effect of matrix properties on dehumidifier performance was examined. The results can also be used to indicate the effect of dehumidifier performance characteristics on the design point performance of a desiccant cooling cycle.

A ventilation cycle (Figure 1.3) operated with a regeneration temperature of 85°C at the SERI standard room and ambient conditions [105] would have dehumidifier inlet states corresponding to the inlet state pair 1 of §4.4. The dehumidifier outlet states calculated using the finite difference solution can be readily applied to estimate the design point performance of the ventilation cycle.

The design point performance of the desiccant cooling cycle can be characterized by the specific cooling capacity (cooling capacity per unit air mass flow rate) and the thermal COP. The total cooling capacity scales directly with air flow rate. Comparison of the specific capacity of two systems gives an indication of the relative flow rates required to obtain a given total capacity, and provides a sense either of the total fan power requirements or of the physical size of the components in the systems. The thermal COP is a measure of the thermal energy input required in the cooling system. In the design point calculations presented here, it is assumed that the sensible heat exchanger has negligible air carry-over and an effectiveness of 0.95, and that the room inlet and exhaust evaporative coolers saturate the air streams.

To facilitate discussion, the matrix property effects discussed in §4.4 are categorized by isotherm shape, maximum water content, sensible and latent heat effects, and equivalent NTU_w effects. The design point specific capacity and thermal COP of the ventilation cycle as a function of μ_K are shown in Figures

4.11.a - 4.14.a and Figures 4.11.b - 4.14.b respectively for each of these four major matrix property groups.

Figures 4.11.a and 4.11.b show the effect of the six isotherm shapes (§4.4.1) on the design point specific cooling capacity and COP of the ventilation cycle. The dehumidifier performance data (Table 4.6) revealed that there are 'unfavorable' isotherm shapes that result in substantially less dehumidification of the process air stream than other 'favorable' isotherms. Similarly, Figure 4.11.a shows that there are two levels of specific capacity associated with isotherm shape. The unfavorable (types 3 and 5) isotherms have a maximum specific capacity about 20% less than that of the favorable (types 1, 2, 4, and linear) isotherms. The type 1 isotherm has the highest maximum specific capacity, but also shows the strongest variation with μ_K . The other favorable isotherms result in nearly equivalent system performance. The type 5 isotherm has the lowest maximum specific capacity. In all cases, maximum specific cooling capacity is obtained at the μ_K resulting in optimum dehumidification, μ_{K_x} .

The variation of COP shown in Figure 4.11.b has several interesting trends. Comparing Figure 4.11.b with Figure 4.11.a, it is observed that the maximum COP is obtained at a μ_K slightly greater than that which results in maximum specific capacity. Furthermore, the decay of COP with μ_K greater than the optimum is much weaker than the corresponding decay of specific capacity. A

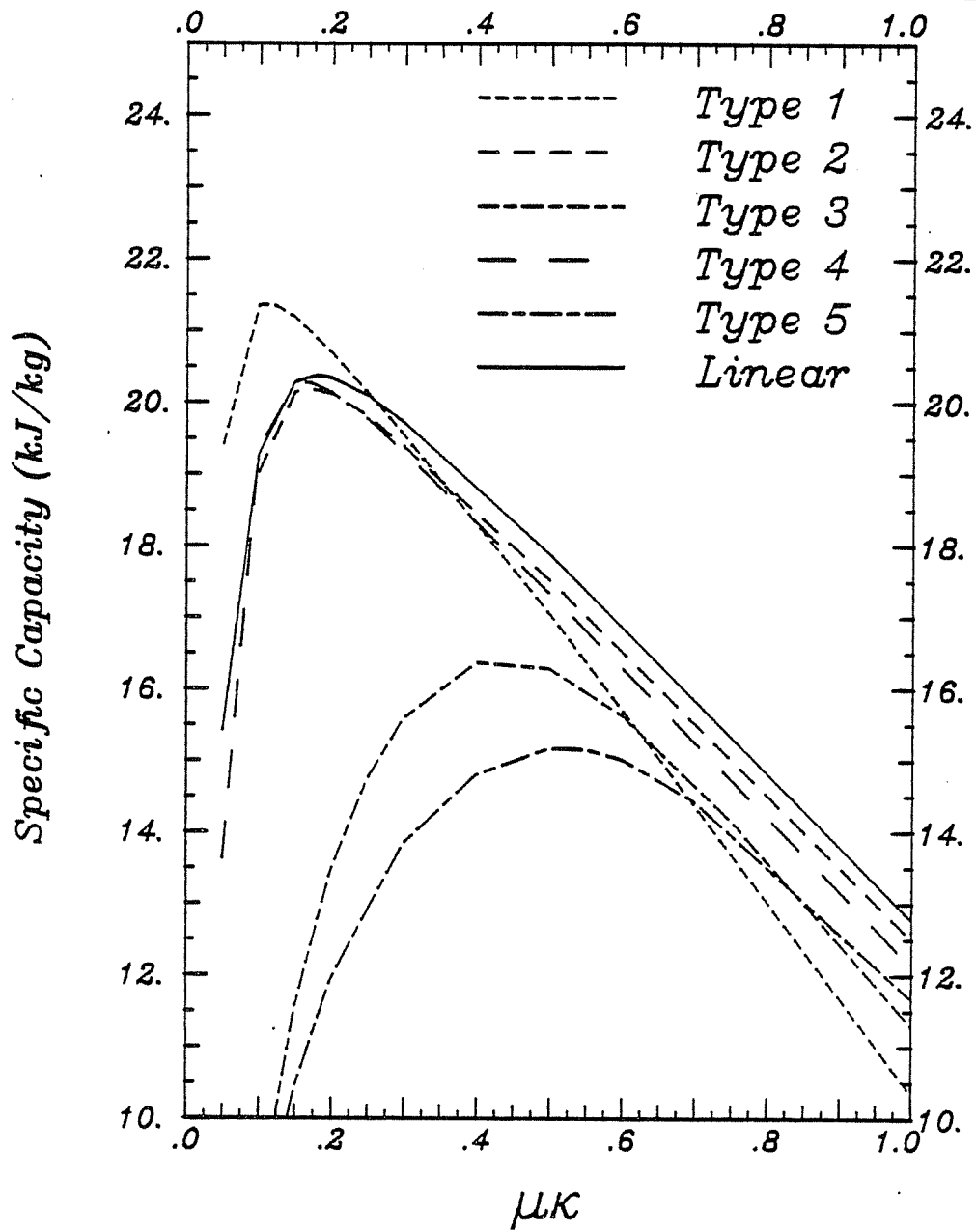


Figure 4.11a Effect of isotherm type on the ventilation cycle specific cooling capacity

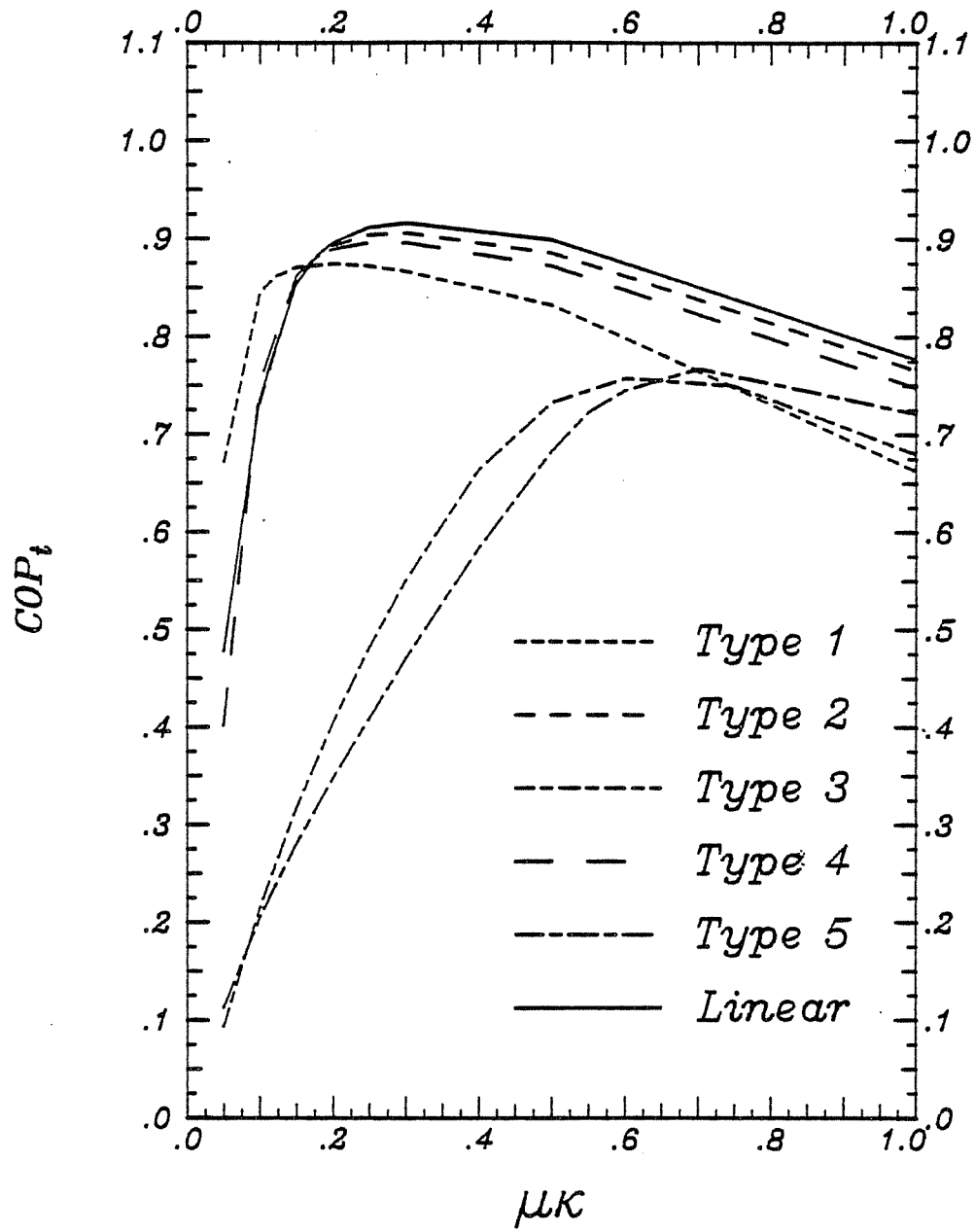


Figure 4.11b Effect of isotherm type on the ventilation cycle COP_t

somewhat surprising result is that the type 1 isotherm, which has the highest maximum specific capacity, has a consistently lower COP than the other favorable isotherms. The type 5 isotherm, which has the lowest specific cooling capacity, has a maximum COP approximately equal to that of the type 3 isotherm. The explanation of these observations share a common foundation.

In this system, which has a high performance heat exchanger, the specific cooling capacity depends primarily on the dehumidifier process stream outlet humidity ratio, and is only secondarily influenced by the outlet temperature. The dehumidifier outlet temperature directly affects the regenerating stream outlet temperature of the sensible heat exchanger, and has an important effect on the thermal energy required to boost the air stream to the regeneration temperature. As shown in Figure 4.10 (§4.4), the dehumidifier outlet temperature and humidity ratio both increase for μK greater than the optimum, and there is a corresponding decrease in both the specific capacity of the cycle and the required thermal energy input. Since the COP is the ratio of cooling capacity to thermal energy input, the compensating changes in both the numerator and denominator of the COP for μK greater than μK_x result in a less pronounced variation with μK than occurs for the specific capacity. The results given in Table 4.6 (§4.4.1) also indicate that at μK_x the type 1 isotherm has the lowest outlet temperature and humidity ratio of the favorable isotherms, while the type 5 isotherm has both the highest outlet temperature and humidity ratio. The high

specific capacity and relatively low COP associated with the type 1 isotherm and the low system specific capacity but relatively high COP obtained with the type 5 isotherm are explained on this basis.

The variation of system specific capacity and COP with $\mu\kappa$ at constant inlet conditions can also have implications for the off--design inlet state operation of the cooling system. Associated with the optimum $\mu\kappa$ at an inlet state are analogous parameters $C_{r,i}^*$ (§3.4). A strong dependence on $\mu\kappa$ at fixed inlet conditions implies a strong variation of performance with dehumidifier $C_{r,i}^*$. But as dehumidifier inlet conditions vary, even though $\mu\kappa$ is fixed, $C_{r,i}^*$ will change. Therefore, if the rotational speed of the matrix is chosen to optimize the performance of the system at design conditions, at off design inlet conditions, the system performance can be substantially degraded, particularly if there is a strong variation in the average analogous capacitance ratios, γ_i , with inlet state. The system results shown in Figures 4.11.a and 4.11.b for the type 1 isotherm, which has a strong performance variation with $\mu\kappa$, can be evaluated in this regard. From Table 4.6, the optimum type 1 $\mu\kappa$ for dehumidification with inlet state pair 2 is 0.22. The design point specific capacity (Figure 4.11.a) evaluated at this $\mu\kappa$ is about 10% less than the maximum. The other materials would show a similar variation from the maximum design point specific capacity if evaluated at the $\mu\kappa_x$ for inlet state pair 2 given in Table 4.6. This suggests that the performance of systems using these materials is probably not strongly influenced

by using the optimum design point rotational speed for off—design point operation.

The system performance results illustrated in Figures 4.11.a and 4.11.b imply that a dehumidifier with a favorable isotherm is preferred. The linear isotherm overall has satisfactory performance.

The effect of the maximum water content of a linear isotherm desiccant on system performance is shown in Figures 4.12.a and 4.12.b. The results show that the $W_{mx} = 0.25$ isotherm results in the lowest maximum specific capacity but highest maximum COP, while the $W_{mx} = 1.0$ isotherm has the greatest maximum specific capacity with the lowest maximum COP. The variation in maximum specific capacity is about 10%, roughly twice the change in maximum COP. In Table 4.6 (§4.4.3), it is observed that the $W_{mx} = 0.25$ isotherm has the highest outlet temperature and humidity ratio, and the $W_{mx} = 1.0$ isotherm has the lowest outlet temperature and humidity ratio of the linear isotherms compared. The explanation of the effect of isotherm variation on system performance can be consistently applied to this case. The performance of the system with the nominal linear isotherm dehumidifier again compares favorably to the performance obtained with $W_{mx} = 1.0$ isotherm regenerator.

The analysis of the effect of large heat of adsorption and large matrix thermal capacitance on dehumidifier performance in §4.4.2 and §4.4.6 demonstrated that these latent and sensible heat phenomena resulted in an increase in dehumidifier outlet temperature

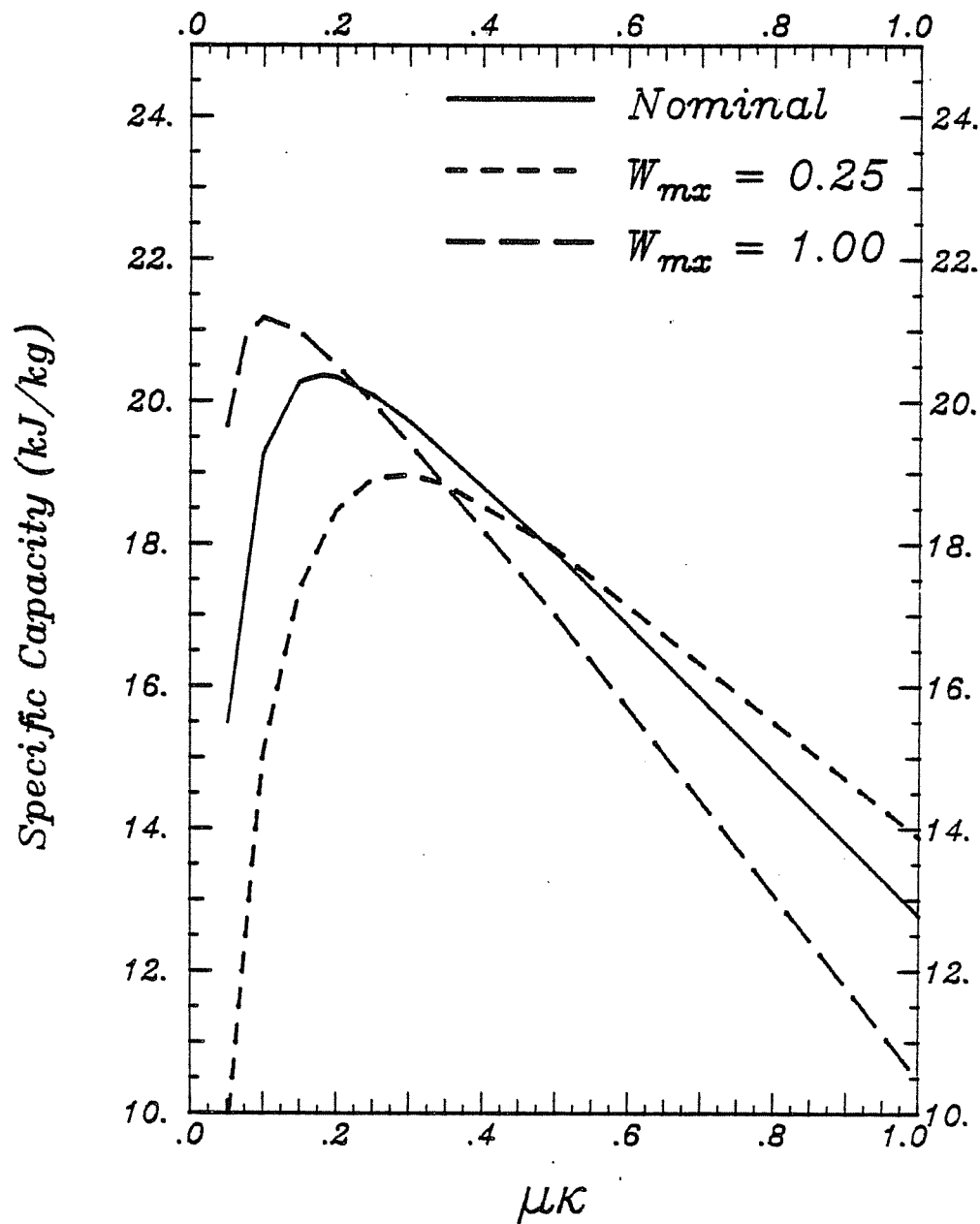


Figure 4.12a Effect of linear isotherm maximum water content on the ventilation cycle specific cooling capacity

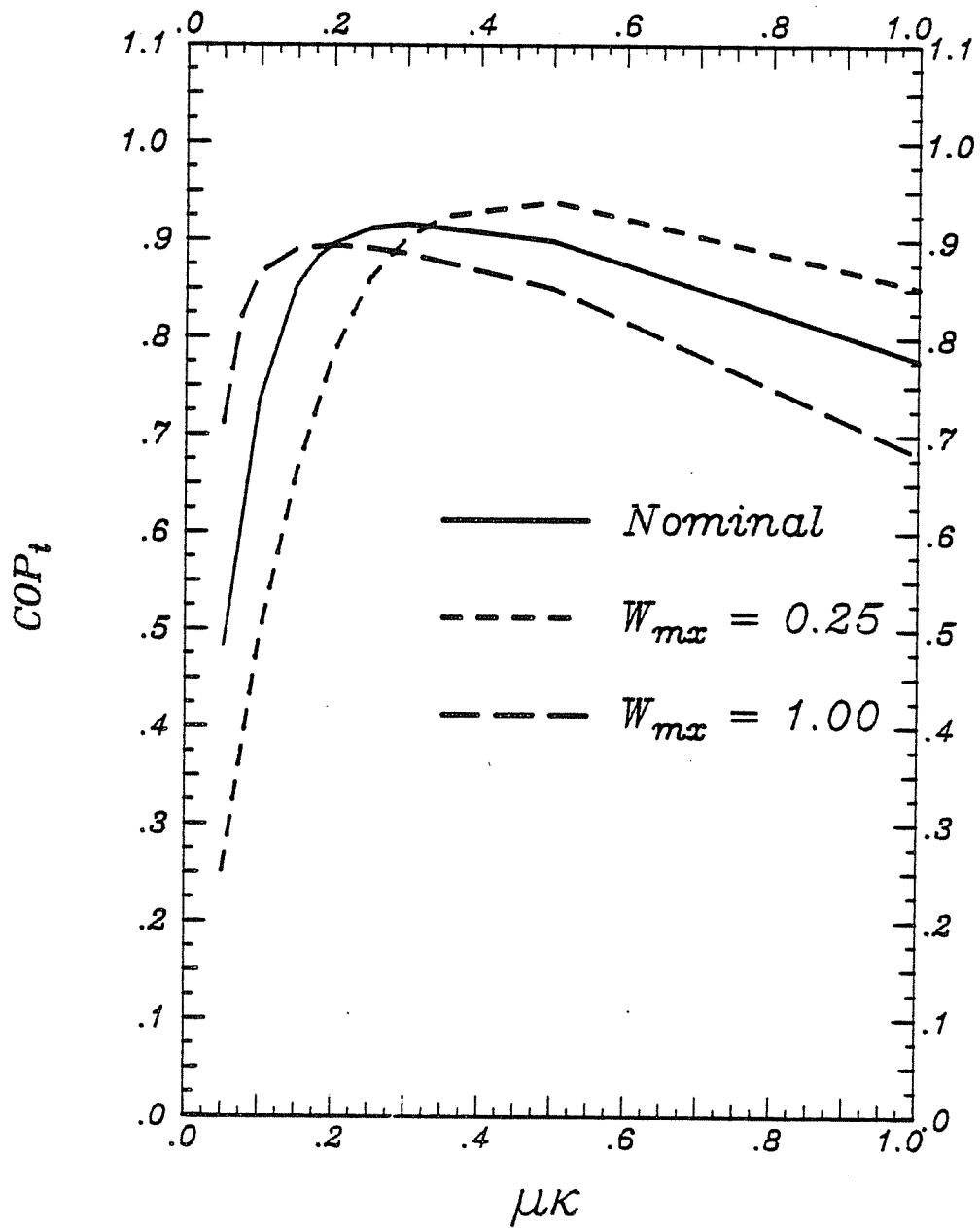


Figure 4.12b Effect of linear isotherm maximum water content on ventilation cycle COP_t

and humidity ratio compared to the outlet states of the nominal linear isotherm dehumidifier. The impact on system performance of this behavior is illustrated in Figures 4.13.a and 4.13.b. The data shown in Figure 4.13.a indicate that the maximum system specific cooling capacity is decreased by about 15% when a large heat of adsorption or large matrix thermal capacitance material is used in place of the nominal linear isotherm desiccant in the dehumidifier. The large thermal capacitance material also shows a very strong dependence on μK compared to other materials. As mentioned previously, this strong dependence on μK may imply that the high thermal capacitance dehumidifier system may be adversely affected by off--design point operation. On the other hand, the large h^* isotherm results in a relatively weak decay in specific capacity for μK greater than μK_x , and the system performance may be fairly insensitive to inlet state.

The effect of large heat of adsorption and thermal capacitance matrix properties on system COP is shown in Figure 4.13.b. The large matrix thermal capacitance system has a maximum COP slightly greater than that of the nominal system, but the decay of COP with μK greater than μK_x is very pronounced. Again, this implies that the optimum system performance occurs only in a very narrow rotational speed range, which is probably dependent on dehumidifier inlet states. The dehumidifier with the large h^* desiccant, on the other hand, results in a maximum COP roughly 15% greater than that of nominal linear isotherm desiccant system. The COP of this

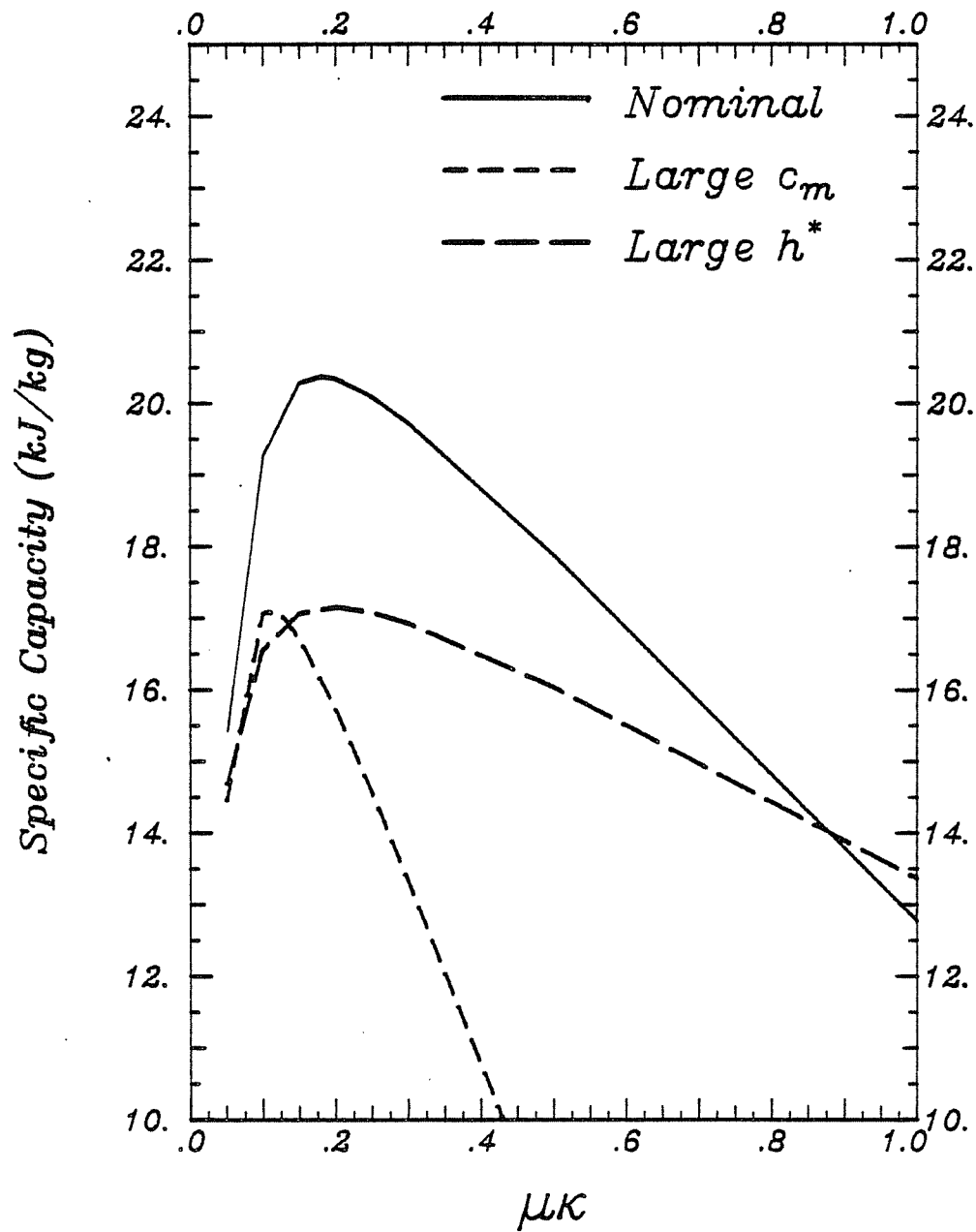


Figure 4.13a Effect of sorption heat phenomena on ventilation cycle specific cooling capacity

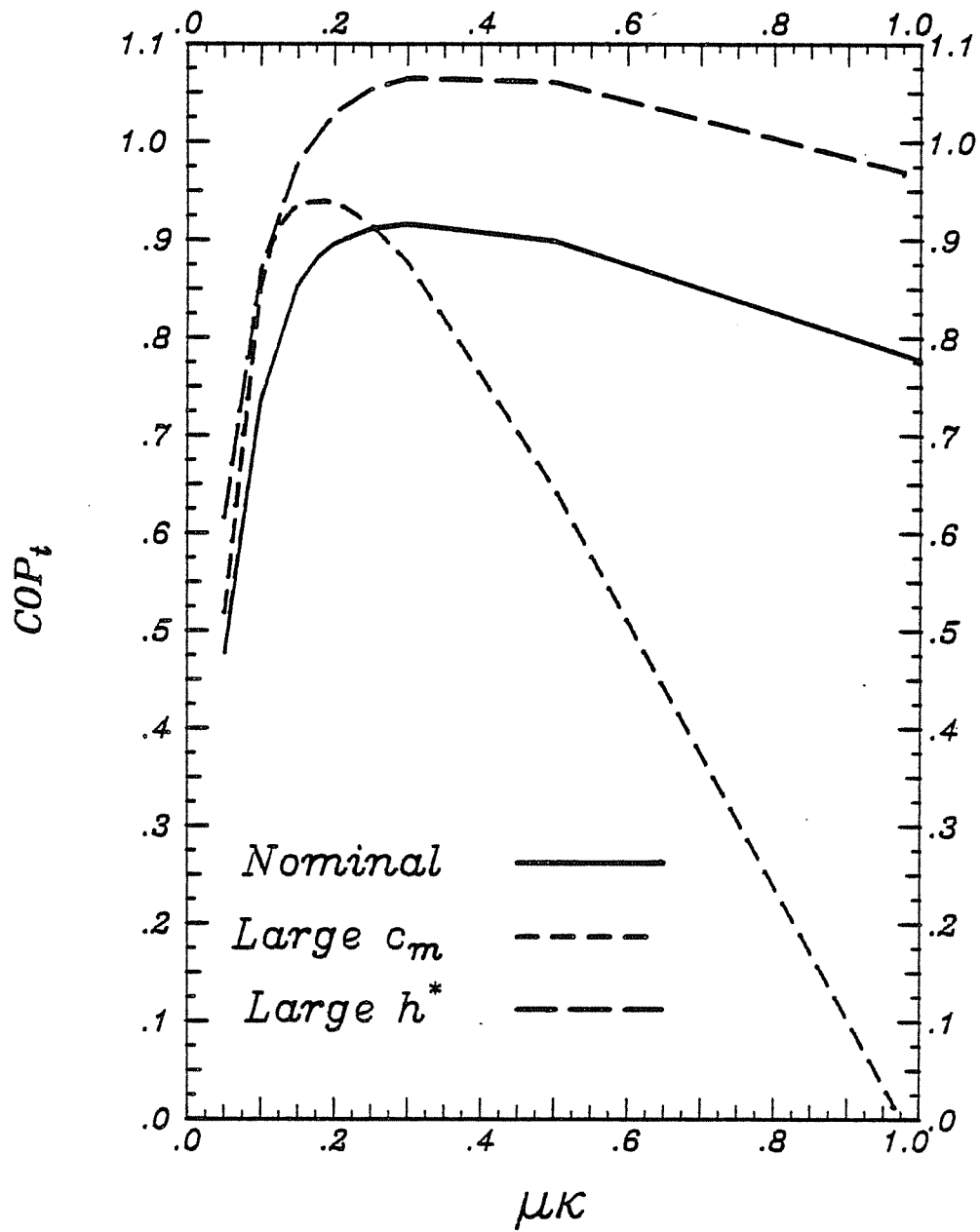


Figure 4.13b Effect of sorption heat phenomena on ventilation cycle COP_t

system is not strongly affected by $\mu\kappa$ greater than $\mu\kappa_x$.

Taken together, the variation of system specific capacity and thermal COP with sensible and latent heat effects suggests that if the air flow rate through the system is unimportant (either the fan power requirements or the physical size of the components are not constrained) then there might be interest in the large h material. However, because of the sensitivity of the large thermal capacitance matrix system to $\mu\kappa$, the utility of this alternative is suspect.

The matrix properties discussed to this point have largely resulted in compromises between system specific capacity and thermal COP. The results shown in Figure 4.14.a and 4.14.b for the hysteresis isotherm and the $Le_o = 4$ dehumidifier indicate that there is no such ambiguity in the effect of decreasing the effective NTU_w of the dehumidifier: both the system specific capacity and COP are significantly degraded. The hysteresis isotherm has a particularly detrimental effect on system performance, resulting in a maximum specific capacity and COP 30% and 50% less than obtained using the nominal linear isotherm dehumidifier.

4.6 Conclusions

The effect of six different matrix properties on the design point performance of a counterflow rotary dehumidifier and a ventilation cycle air conditioner has been investigated. The

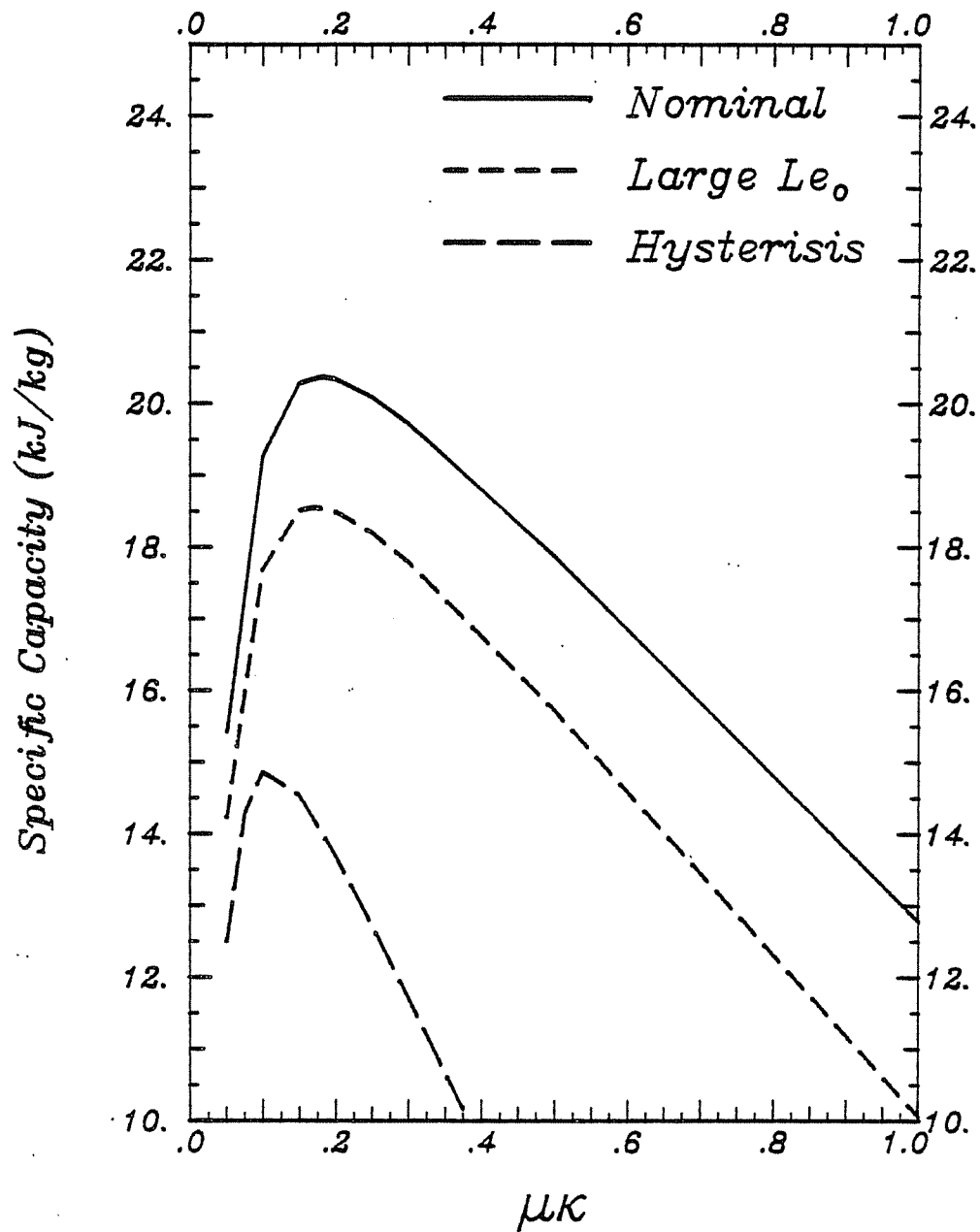


Figure 4.14a Effect of low mass transfer phenomena on ventilation cycle specific cooling capacity

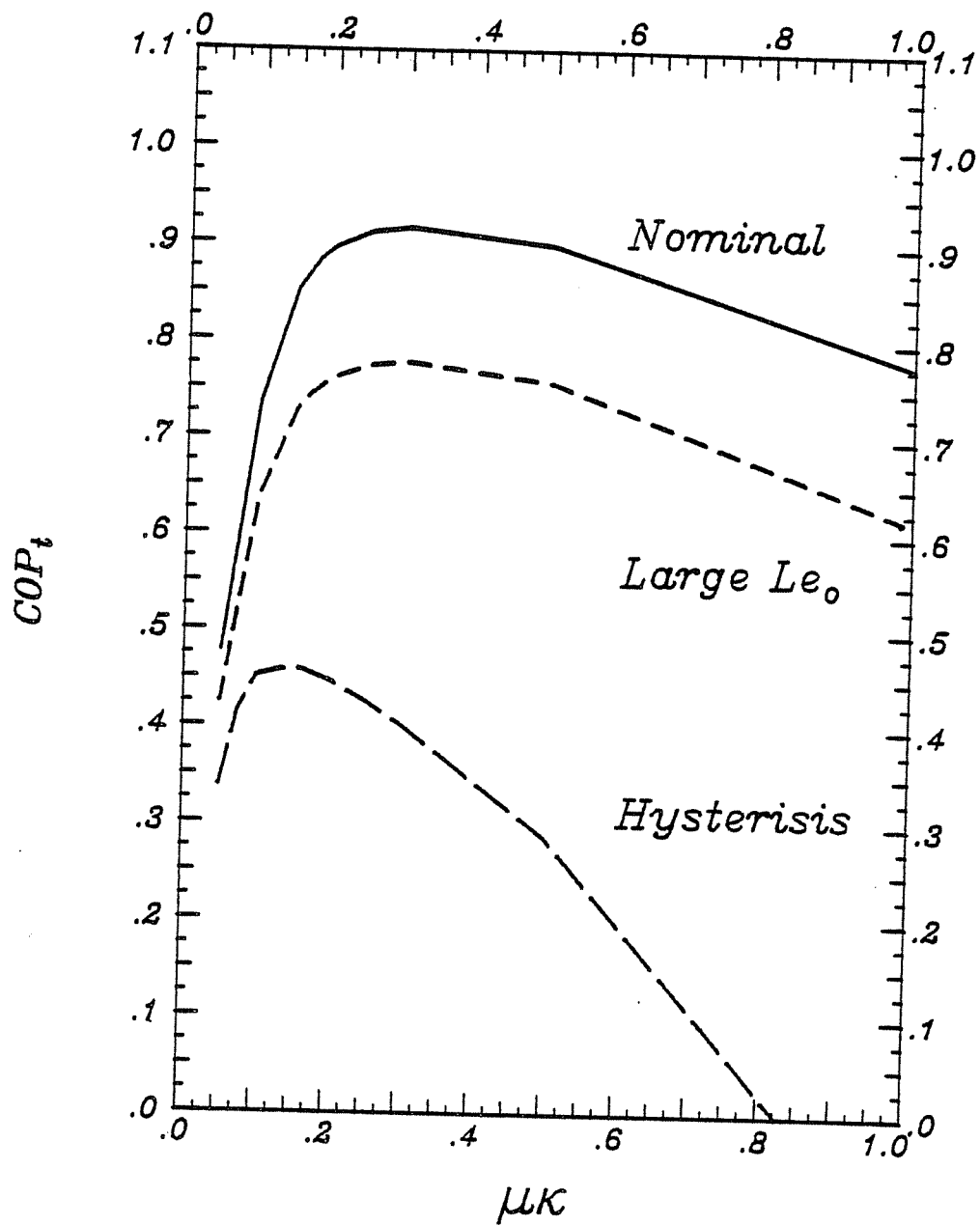


Figure 4.14b Effect of low mass transfer phenomena on ventilation cycle COP_t

properties considered have been isotherm shape, heat of adsorption, maximum water content, adsorption hysteresis, matrix moisture diffusivity and matrix thermal capacitance. Results have been obtained for the maximum dehumidification efficiency and the air conditioning system specific cooling capacity and thermal COP in each case. The dehumidifier performance results are reviewed first, and subsequently the design point performance of the ventilation cycle is discussed.

The nominal desiccant employed in this study had a linear isotherm with $W_{mx} = 0.5$, and a heat of adsorption and thermal capacitance similar to silica gel. The only perturbations that consistently improve the dehumidifier performance over this base case are changing the isotherm shape to type 1 and increasing the maximum water content to $W_{mx} = 1.0$. The type 1 isotherm with $W_{mx} = 0.5$ results in better dehumidifier performance than does the linear isotherm with $W_{mx} = 1.0$.

Several property changes result in little net change in dehumidifier performance compared to the nominal linear isotherm. These include using adsorbents with type 2 or type 4 isotherms (with $W_{mx} = 0.50$) and decreasing the heat of adsorption for the linear isotherm to be identically the heat of vaporization of water ($\Delta h^* = 0$).

The other perturbations resulted in a decrease in dehumidifier performance. Decreasing W_{mx} to 0.25 for the linear isotherm had the least detrimental effect, followed by increasing Le_o from 1.0

to 4.0. Increasing the heat of adsorption, so that the linear isotherm was strongly temperature dependent, and increasing the matrix thermal capacitance by a factor of 3.5 had roughly equivalent adverse effect on the maximum dehumidification. The worst dehumidifier performance was obtained with the type 3, type 5, and the hysteresis isotherms. These cases resulted in maximum dehumidifier efficiencies η_{wx} approximately 25% below that obtained with nominal linear isotherm.

Since both isotherm shape and maximum water content were found to affect dehumidifier performance, a molecular sieve with $W_{mx} = 0.25$, a microporous silica gel with $W_{mx} = 0.50$, and a macroporous silica gel with $W_{mx} = 1.125$ were modeled. The microporous adsorbent resulted in substantially better dehumidifier performance than did the other materials.

The variation of matrix properties has a profound effect on the design requirements for high performance dehumidifiers. For example, the dehumidifier NTU_0 required for a given level of performance can vary by a factor greater than four as the shape of the adsorption isotherm changes.

The results of this investigation can be summarized in several rough guidelines. For maximum dehumidifier performance, an adsorbent with a near type 1 isotherm similar to those characteristic of microporous adsorbents should be selected. If an alternate isotherm is considered the maximum water content must be substantially greater than that of the type 1 adsorbent to realize equi-

valent dehumidifier performance. The heat of adsorption of the material should be low. It is preferable to design a matrix with low thermal capacitance and $Le_0 > 1$ than to have very high matrix thermal capacitance and $Le_0 = 1$. Isotherms with significant hysteresis loops should be avoided.

The results of the design point study of the ventilation cycle closely mirror the results of dehumidifier performance investigation. The only perturbations which result in a significant increase in the maximum specific cooling capacity of the cycle over that obtained with the nominal linear isotherm dehumidifier are employing the type 1 microporous adsorbent and increasing the linear isotherm W_{mx} to 1.0. Both of these changes result in maximum COP less than obtained with the nominal isotherm. The only change in matrix properties which resulted in a significant increase in COP compared to the nominal case was to use an adsorbent with a large heat of adsorption. However, the maximum specific capacity of this system was significantly less than that of the nominal system. There were no changes which resulted in a simultaneous increase in system cooling capacity and COP. However, both an $Le_0 > 1$ and a hysteresis isotherm dehumidifier resulted in a simultaneous degradation of system cooling capacity and COP.

Cumulatively, these guidelines suggest that commercially available microporous silica gels are attractive materials for

dehumidifier construction. Radical changes in desiccant properties would be required to significantly improve dehumidifier or cooling system performance over that obtainable with these materials.

CHAPTER 5

THE EFFECT OF MATRIX PROPERTIES ON THE ACCURACY
OF THE INTERSECTION POINT METHOD

The analogy solutions were shown in Chapter 3 to accurately predict the outlet states of a high performance silica gel dehumidifier. It is of interest to determine the extent to which the matrix property variations analysed in Chapter 4 affect the accuracy of these approximate solutions. However, to provide a parallel comparison of the intersection point and nonlinear analogy methods similar to that made in Chapter 3 would require that F_i curve fits be determined for each property set. This is a formidable task that, for present purposes, is unnecessary. The results in Chapter 3 suggest that while the errors in the two analogy methods can be attributed to different approximations inherent in the solutions, they are nonetheless of the same order of magnitude. While there are reasons to believe that one or the other method might work somewhat better for a given property set, it is difficult to argue that the errors in the two solutions would ever differ by an order of magnitude. Therefore, the intersection point method, which is easily adapted to handle different matrix properties, was used to indicate the accuracy of the analogy solutions when applied to the various property sets.

The intersection point method was used to predict the dehumidifier outlet states for each of the property sets discussed

in Chapter 4. With the exception of the hysteresis isotherm, for which the combined F_i potentials can't be defined [28]. Rather than repeat the sequential development of Chapter 4 here in the context of the analogy solution, detailed results will be presented for only two matrix property sets. Because a matrix with a type 1 adsorbent is desirable, and practical experience shows that a large matrix thermal capacitance may be unavoidable [56], the intersection point method results are discussed for these two matrix property sets. The remainder of the results are summarized, though all of the error data is provided in an appendix for an interested reader.

5.1 Property Dependent Variations of the F_i and γ_i

All of the matrix properties except Le_o affect both the α_i (Eqs. (3.8)) and the γ_i (Eqs. (3.9)). It is convenient to discuss these quantities in terms of their representation on a psychrometric chart. Banks [28] has shown that as the isotherm slope increases, α_1 and α_2 tend to α_a and α_r (Eqs. 3.10) respectively, so that the F_1 and F_2 lines will tend to parallel adiabatic saturation temperature and relative humidity lines. An increase in isotherm slope also increases the γ_i . As the matrix thermal capacitance or the heat of adsorption increases, the F_1 lines flatten, and tend toward humidity ratio lines, while the F_2 lines steepen, and tend toward temperature lines. Increasing the matrix thermal

capacitance significantly increases γ_1 without greatly changing γ_2 . A large increase in the heat of adsorption increases γ_2 and decreases γ_1 .

The F_i and γ_i lines for the type 1 isotherm and the large thermal capacitance linear isotherm are shown in Figures 5.1 through 5.4 superimposed on the F_i and γ_i lines for the nominal silica gel (Table 4.1). Figure 5.1 shows that at high relative humidity, where the type 1 isotherm is flat, the type 1 isotherm F_1 lines are slightly flatter than the nominal silica gel F_1 , while the type 1 F_2 lines are steeper than their nominal counterparts. At low relative humidity, the type 1 F_i lines more closely parallel wet bulb temperature and relative humidity lines than do the F_i for the nominal silica gel. The deviations of the type 1 F_i from the nominal F_i are more pronounced at low relative humidity. The type 1 γ_i shown in Figure 5.2 do not exhibit the monotonic variation at constant temperature or humidity ratio of the nominal γ_i . Also, comparing Figures 5.1 and 5.2, it is evident that there is a much greater difference in the shapes of the F_i and γ_i curves for the type 1 isotherm than for the nominal silica gel. As mentioned in §3.3, this implies that the F_i equations for the regenerator (Eqs. (3.14)) are more strongly coupled than in the nominal case, and should have a bearing on the accuracy of the approximate solution.

Figures 5.3 and 5.4 show the F_i and γ_i for the high thermal capacitance linear isotherm. The large matrix thermal capacitance results in flatter F_1 and steeper F_2 lines than are obtained with

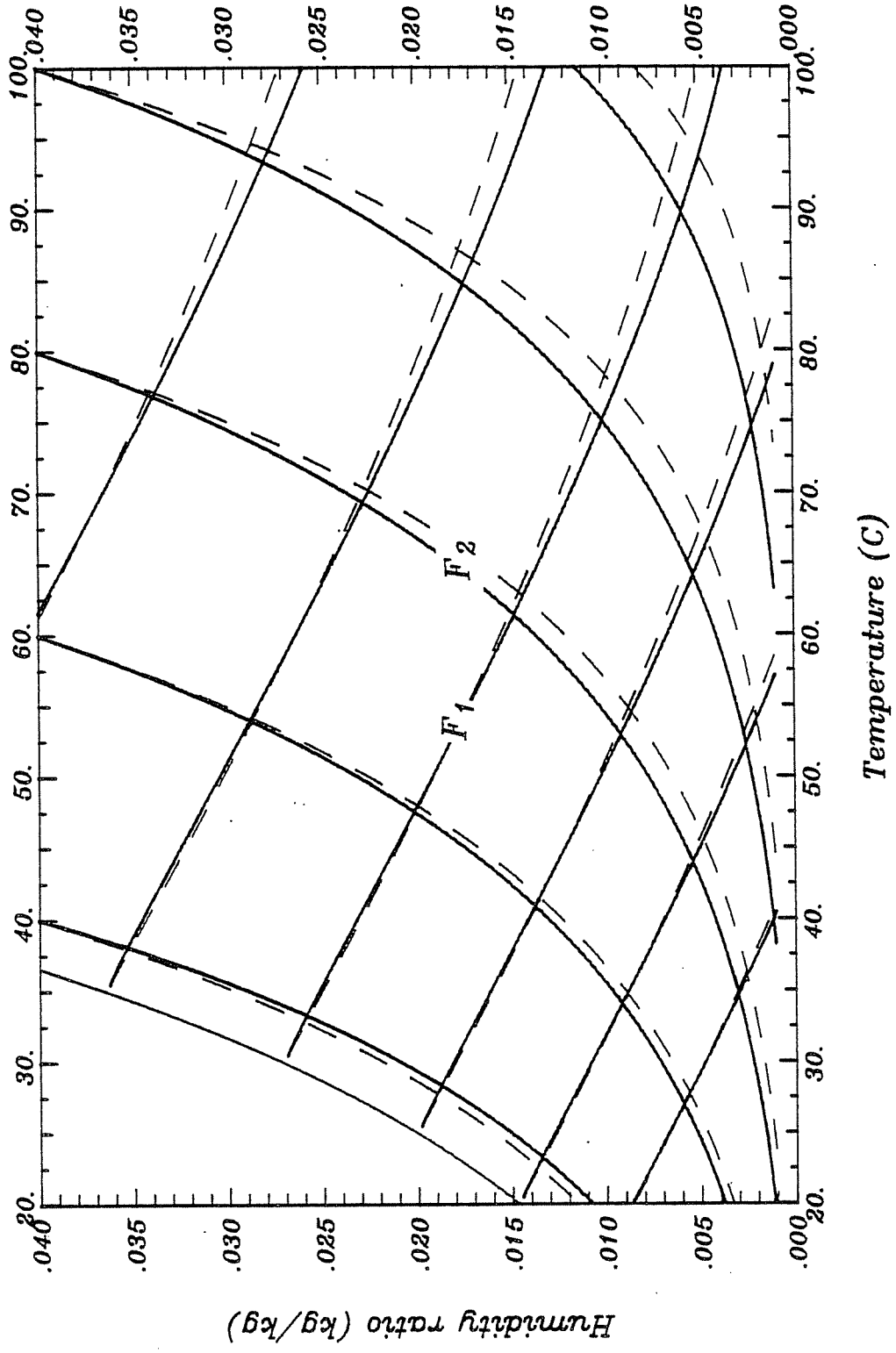


Figure 5.1 F_i potentials for the type 1 isotherm superimposed on the nominal silica gel F_i

Temperature (C)

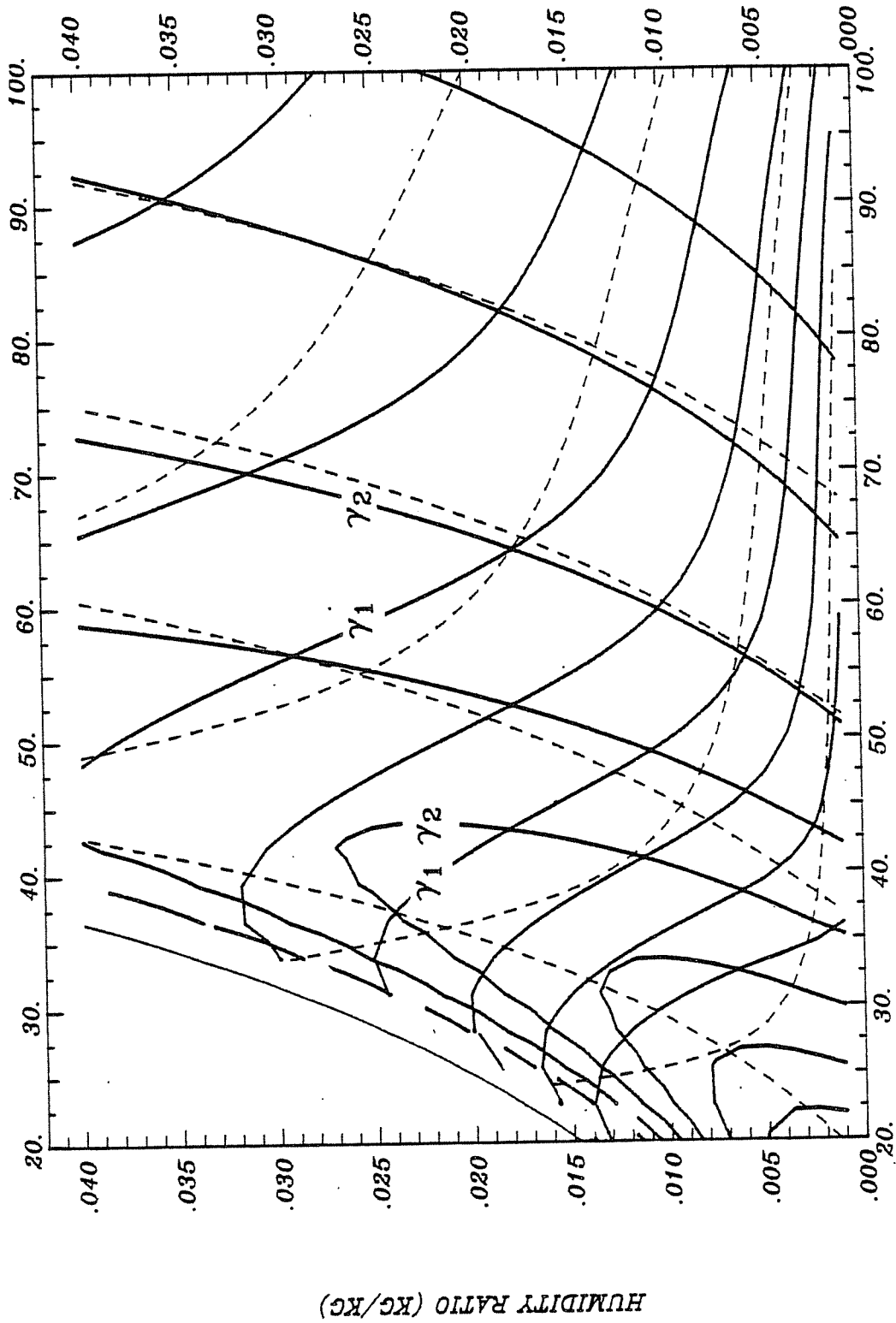


Figure 5.2 γ_i for the type 1 isotherm superimposed on the nominal silica gel γ_i

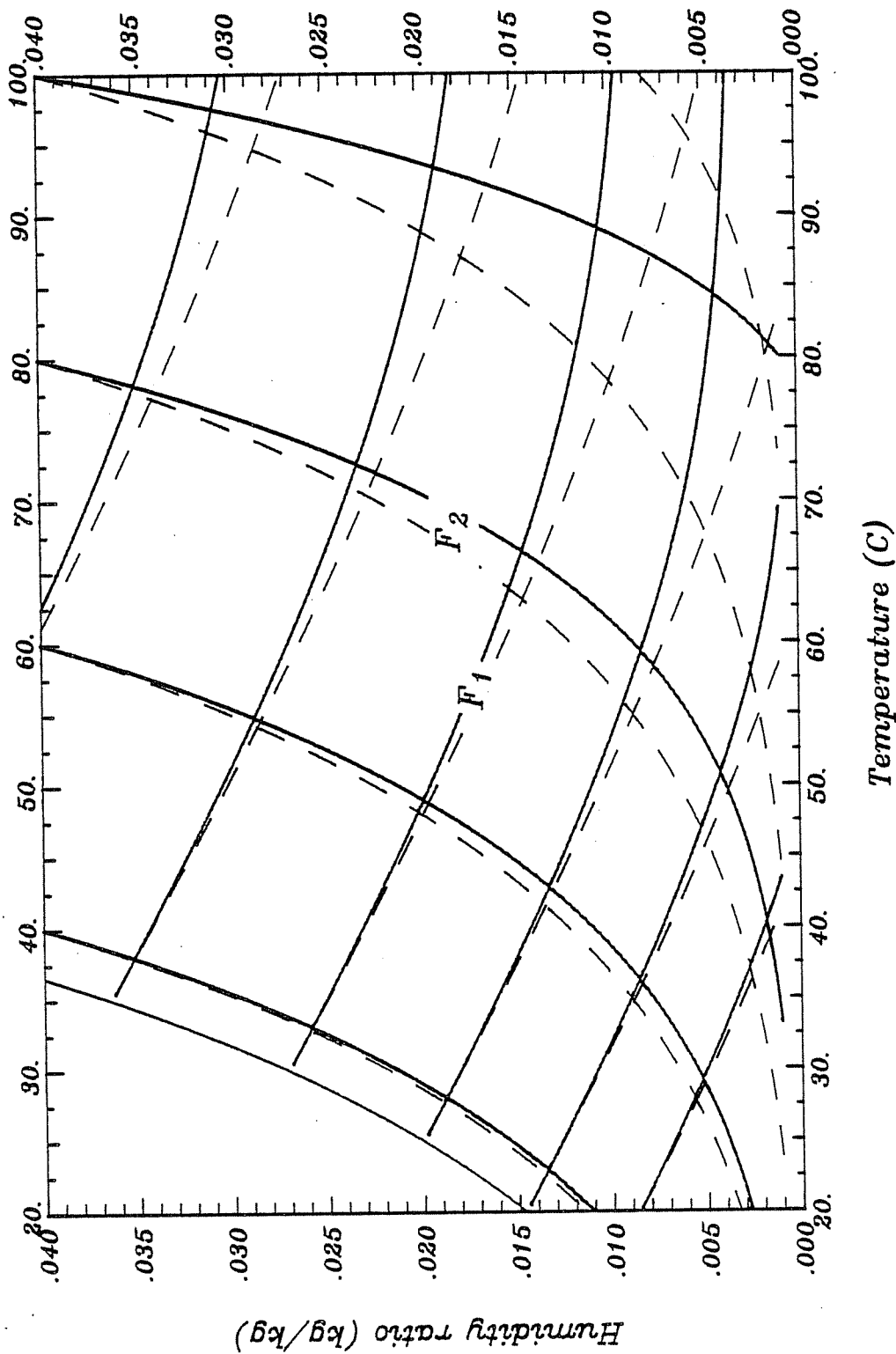
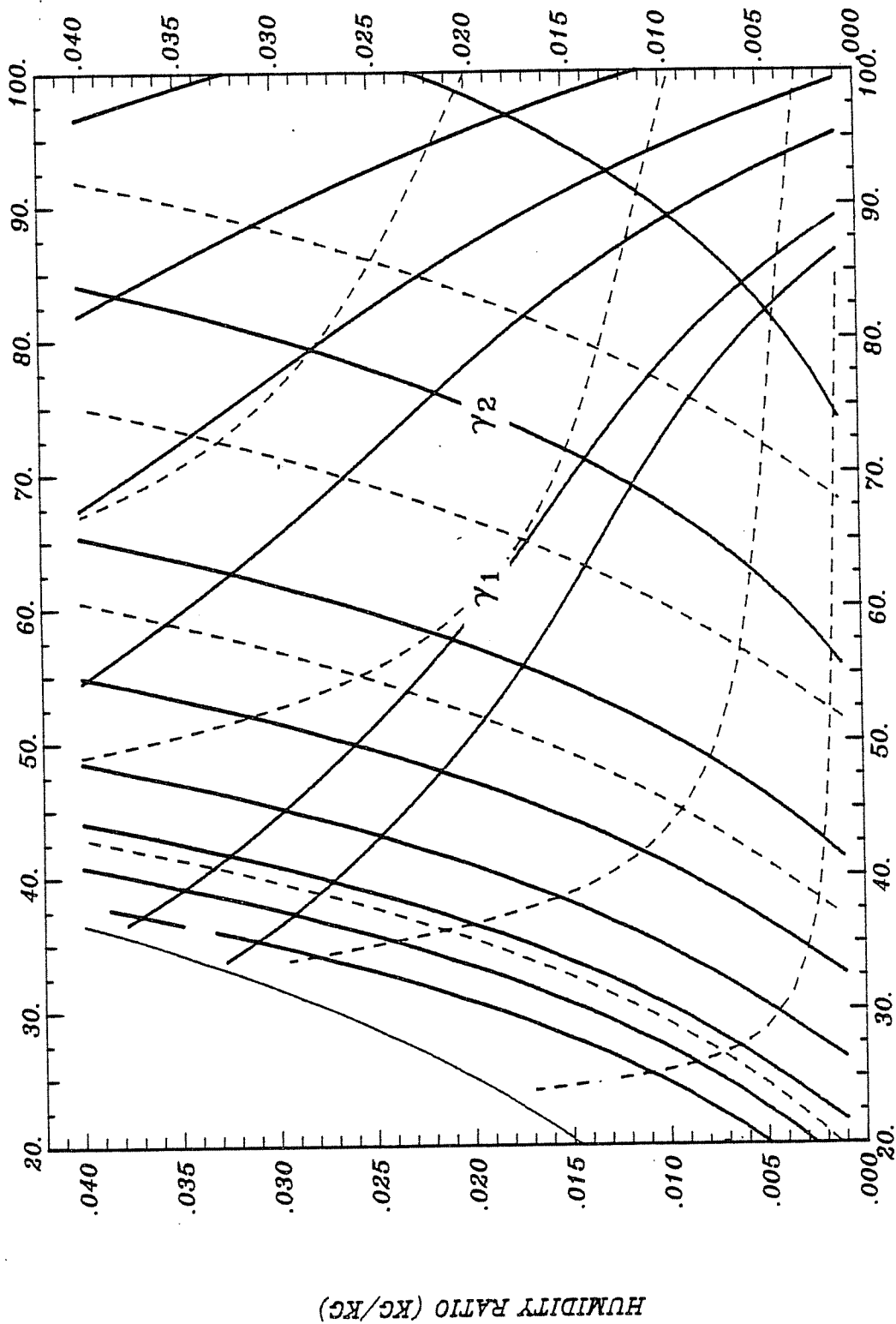


Figure 5.3 F_i potentials for the large thermal capacitance linear isotherm superimposed on the nominal silica gel F_i

Temperature (C)



TEMPERATURE (C)

Figure 5.4 γ_1 for the large thermal capacitance linear isotherm superimposed on the nominal silica gel γ_1

the nominal silica gel. The large thermal capacitance increases γ_2 without greatly changing the dependence of γ_2 on air temperature and humidity ratio, but nearly doubles the values of γ_1 and also affects the variation of γ_1 with air state.

A survey of the F_i diagrams for the other isotherms shows that the F_i for the type 2, type 4 and type 4a isotherms show somewhat less deviation from the nominal silica gel F_i than do those for the type 1 isotherm. The types 3, 5 and 1a isotherm F_i vary substantially from the nominal case. The linear isotherm with $W_{mx} = 0.25$ has F_i similar to those of the large thermal capacitance isotherm, though the magnitude of the variation from the nominal case is less. The linear $W_{mx} = 1.0$ isotherm has F_i that more closely parallel wet bulb temperature and relative humidity ratio lines than those for the nominal case.

The γ_i for the other matrix properties show considerable deviation from the regular behavior of the γ_i for the nominal case. The types 2, 3, $W_{mx} = 0.25$ and $W_{mx} = 1.0$ isotherms all have variations in γ_i with air state roughly similar to that of the nominal silica gel γ_i , though the values are different. The type 4, type 4a and type 5 isotherms γ_i resemble the type 1 γ_i , though the local maximum in γ_2 shown in Figure 5.2 for the type 1 isotherm is much more evident for these materials. The types 2 and 3 and the linear isotherms have γ_i lines that at least resemble their respective F_i lines; the others have γ_i that deviate strongly from the F_i .

5.2 Numerical Results

Tables 5.1 and 5.2 list the process air stream outlet states and the differences between the analogy and exact solution for the type 1 and high thermal capacitance linear isotherms. Data are given for the nominal balanced and symmetric counterflow $Le_o = 1.0$, $NTU_o = 10.0$ dehumidifier for both inlet states employed in Chapter 4. To facilitate comparison, data for a comparable nominal silica gel dehumidifier are given in Table 5.3.

The error data in Table 5.1 indicate that the analogy solution is quite accurate for the type 1 isotherm. The errors in outlet temperature and humidity ratio over most of the $\mu\kappa$ ranges shown are at least as small as those for the nominal silica gel at near optimum $\mu\kappa$. The intersection point method underpredicts the outlet temperature by about 0.2°C and overpredicts the outlet humidity ratio by about 0.2 g/kg for most of the $\mu\kappa$ range for inlet state 1. The large error at $\mu\kappa = 0.05$ is associated with $C_{r,2}^* \approx 1.5$, which is close to unity. The intersection point method predictions for the type 1 isotherm dehumidifier with inlet state pair 2 show about half the error of the corresponding solution for the nominal silica gel dehumidifier. Except for $\mu\kappa \leq 0.15$, which are associated with the transition from low to medium rotational speed ($C_{r,2}^*$ near unity), the inlet state 2 type 1 isotherm errors are about 0.4°C and 0.2 g/kg .

Table 5.1 Finite difference solution for the process outlet states of a type 1 isotherm dehumidifier and the errors in the outlet states predicted by the intersection point method

	t (°C)	w (g/kg)
process:	35.000	14.200
regeneration:	85.000	14.200
inter. pt.:	63.141	3.864

$\mu\kappa$	t (°C)	w (g/kg)	Δt (°C)	Δw (g/kg)
.050	59.544	5.581	2.512	-.851
.100	63.337	4.739	.244	-.089
.120	63.838	4.729	.041	.003
.150	64.360	4.792	-.088	.078
.200	65.031	4.972	-.161	.158
.250	65.599	5.181	-.160	.219
.300	66.134	5.402	-.140	.268
.500	68.171	6.340	-.010	.430
1.000	72.985	8.881	.366	.709
5.000	80.195	13.958	-.132	.052

	t (°C)	w (g/kg)
process:	30.000	24.500
regeneration:	100.000	14.200
inter. pt.:	83.779	5.042

$\mu\kappa$	t (°C)	w (g/kg)	Δt (°C)	Δw (g/kg)
.050	69.669	9.883	8.233	-2.523
.100	77.664	7.626	3.242	-1.062
.150	80.374	7.046	1.249	-.477
.200	81.673	6.918	.377	-.241
.220	82.030	6.918	.162	-.188
.250	82.473	6.947	-.086	-.132
.300	83.062	7.047	-.376	-.079
.500	84.699	7.698	-.948	-.077
1.000	87.658	9.689	-1.443	-.365
5.000	93.282	14.889	-.146	.022

Table 5.2 Finite difference solution for the process outlet states of a large thermal capacitance dehumidifier and the errors in the outlet states predicted by the intersection point method

	t (°C)	w (g/kg)
Process:	35.000	14.200
regeneration:	85.000	14.200
inter. pt.:	75.373	3.815

$\mu\kappa$	t (°C)	w (g/kg)	Δt (°C)	Δw (g/kg)
.050	60.472	7.511	8.105	-1.457
.100	68.638	6.322	3.954	-.611
.115	69.597	6.285	3.352	-.485
.125	70.065	6.299	3.076	-.429
.150	70.920	6.411	2.615	-.342
.200	72.030	6.780	2.109	-.268
.250	72.840	7.222	1.800	-.242
.300	73.537	7.696	1.562	-.236
.500	75.906	9.657	.872	-.244
1.000	79.262	12.941	.145	.012
5.000	80.421	14.136	-.018	.010

	t (°C)	w (g/kg)
process:	30.000	24.500
regeneration:	100.000	14.200
inter. pt.:	97.332	7.785

$\mu\kappa$	t (°C)	w (g/kg)	Δt (°C)	Δw (g/kg)
.050	69.203	13.020	19.485	-2.882
.100	81.415	11.027	9.954	-1.299
.125	70.065	6.299	3.076	-.429
.150	85.917	10.456	6.009	-.612
.170	86.772	10.409	5.274	-.494
.200	87.649	10.418	4.529	-.384
.250	88.570	10.543	3.762	-.296
.300	89.179	10.731	3.266	-.261
.500	90.617	11.694	2.139	-.295
1.000	92.557	13.947	.709	-.349
5.000	93.507	15.115	.003	-.027

Table 5.3 Finite difference solution for the process outlet states of the nominal silica gel dehumidifier and the errors in the outlet states predicted by the intersection point method.

	t (°C)	w (g/kg)
process:	35.000	14.200
regeneration:	85.000	14.200
inter. pt.:	65.514	3.846

$\mu\kappa$	t (°C)	w (g/kg)	Δt (°C)	Δw (g/kg)
.010	40.002	12.465	.206	.000
.050	54.610	7.696	4.939	-1.529
.100	61.633	5.834	3.014	-.997
.150	64.660	5.257	.907	-.386
.200	65.956	5.167	.170	-.123
.250	66.692	5.242	-.100	-.002
.300	67.236	5.374	-.215	.072
.500	68.901	6.069	-.291	.247
1.000	72.313	8.003	.041	.557
5.000	80.077	13.857	-.198	.034

	t (°C)	w (g/kg)
process:	30.000	24.500
regeneration:	100.000	14.200
inter. pt.:	87.146	5.361

$\mu\kappa$	t (°C)	w (g/kg)	Δt (°C)	Δw (g/kg)
.050	62.056	13.075	17.201	-4.937
.100	72.217	10.230	11.297	-3.149
.150	77.800	8.914	6.573	-1.841
.200	80.831	8.264	4.006	-1.072
.250	82.474	7.992	2.709	-.642
.300	83.494	7.893	1.984	-.369
.500	85.480	8.104	1.005	.174
1.000	87.784	9.427	.957	.815
5.000	93.228	14.802	-.253	-.050

In contrast to the results for the type 1 isotherm, the data in Table 5.2 show that the intersection point method does not accurately predict the outlet states for the high thermal capacitance linear isotherm dehumidifier. The dehumidifier performance is consistently overpredicted by the intersection point method. The error in the outlet temperature is about 2°C over most of the μK range for both inlet states. The outlet humidity ratio is consistently underestimated by about 0.3 g/kg. These errors are due primarily to a substantial overestimation of the F_2 efficiency of the dehumidifier, which corresponds to a large overestimation of the average γ_2 .

The intersection point method results for the other matrix property sets show a wide variation in accuracy. By far the worst results are obtained for the types 3 and 5 isotherms, where without qualification it can be stated that the approximate solution fails. However, these unfavorable isotherms would almost certainly not be considered for dehumidifier construction, so the poor accuracy of the method for these materials is probably not important. As shown above, the method also does not work well for systems with large thermal capacitance. The results for the linear isotherm with $Le_0 = 4$ show somewhat larger errors in the analogy solution than occur for the large thermal capacitance case. The results for the $W_{mx} = 0.25$ linear isotherm and for the macroporous silica gel (type 4a) isotherm show errors of the same magnitude as for the large thermal

capacitance linear isotherm. A number of materials show analogy method errors roughly similar to those of the nominal silica gel. These include the type 2, type 4, linear isotherm with $W_{mx} = 1.0$, and molecular sieve (type 1a) isotherms. For all of these materials, the errors in the intersection point method predictions for inlet state pair 2 are twice those for inlet state pair 1. This is due to the large difference in the inlet states in the former case, and the typically strong variation of the γ_i at high relative humidity. The intersection point method results for the type 1 isotherm show the least error.

Using the desiccant air conditioner model described in §3.5.7, the operation of ventilation cycle cooling systems with a type 1 isotherm dehumidifier and a large thermal capacitance linear isotherm dehumidifier were simulated for the Miami cooling season. The load and system parameters used in §3.5.7 were employed in these simulations, except that the rotational parameter μ_K was constrained to be at most 0.20. The results presented in §4.4 suggest that restricting μ_K to be between 0.10 and 0.20 should result in near optimum performance for both dehumidifiers. The finite difference and intersection point method models of the dehumidifier were both used for each dehumidifier property set. To reduce computational cost, a two grid size finite difference dehumidifier model (§2.4.3) was used instead of the three grid size method previously employed. The simulation results are presented in Table 5.4.

Table 5.4 Results of six-month Miami cooling season simulations of the ventilation cycle based on finite difference and analogy models of a dehumidifier composed of a type 1 or a large thermal capacitance linear isotherm material

matrix	dh model	COP_t	COP_e
type 1	intersection point	0.79	19.1
	finite difference	0.81	19.3
large C_m	intersection point	0.91	13.9
	finite difference	0.72	12.9

The finite difference model simulation results for the type 1 isotherm dehumidifier indicate that the cooling season average COP_t is 0.79 and the COP_e is 19.1. This performance is similar to that obtained with the nominal silica gel. The intersection point method underpredicts the system COP_t and COP_e by 2% and 1% respectively, a level of error comparable to that observed in the nominal case.

The finite difference solution shows that the large thermal capacitance dehumidifier produces a seasonal COP_t of 0.72 and a COP_e of 12.9. The intersection point method greatly overpredicts the performance of the ventilation cycle with a large thermal capacitance dehumidifier, with an error in COP_t of nearly 25%. The large overestimation of COP_t in this case is due to the consistent overestimation of the dehumidifier process stream outlet air temperature.

5.3 Conclusions

The intersection point method is reasonably accurate when applied to high performance (large NTU_o , $Le_o = 1$) dehumidifier with a matrix formed of a low thermal capacitance material with a favorable adsorption isotherm. Increasing either the matrix thermal capacitance or the overall Lewis number has a detrimental effect on the accuracy of the analogy solution for the dehumidifier process stream outlet state. For example, an intersection point method model of a large thermal capacitance dehumidifier results in a 25% overprediction

of the seasonal COP_t of a ventilation cycle desiccant cooling system. Unfortunately, state of the art dehumidifiers are characterized by significant thermal capacitance of the carrier material and by Le_0 substantially above unity. Application of the current analogy solutions to these devices will result in a significant over estimation of the dehumidifier performance.

CHAPTER 6
RECIRCULATION OF PURGED FLOW IN A
COUNTERFLOW ROTARY DEHUMIDIFIER

In Chapter 4, an attempt was made to improve dehumidifier performance by varying the matrix properties. Another method of improving dehumidifier performance is suggested by the circumferential distribution of air temperature and humidity ratio in the process outlet air stream shown in Figure 6.1. Part of the dehumidified process air stream is considerably hotter and wetter than the mean outlet state. If this hot and wet air is physically separated from the rest of the dehumidified air stream before mixing occurs, the mean temperature and humidity ratio of the process outlet air stream are lowered. The purged air stream may be discarded, but since it is at high temperature it can be recirculated and used in the regenerating period. The recirculated purge stream may either be mixed with the bulk regenerating stream or used to produce a locally nonuniform inlet distribution in the regenerating period inlet. The purge and recirculation of part of the dehumidifier air flow can increase the dehumidification in the process stream and decrease the energy input to the regenerating stream.

The recirculated purge dehumidifier with a spatially nonuniform regenerating stream inlet state is analysed in this chapter. An equilibrium analysis of the dehumidifier (§3.3) is first used to

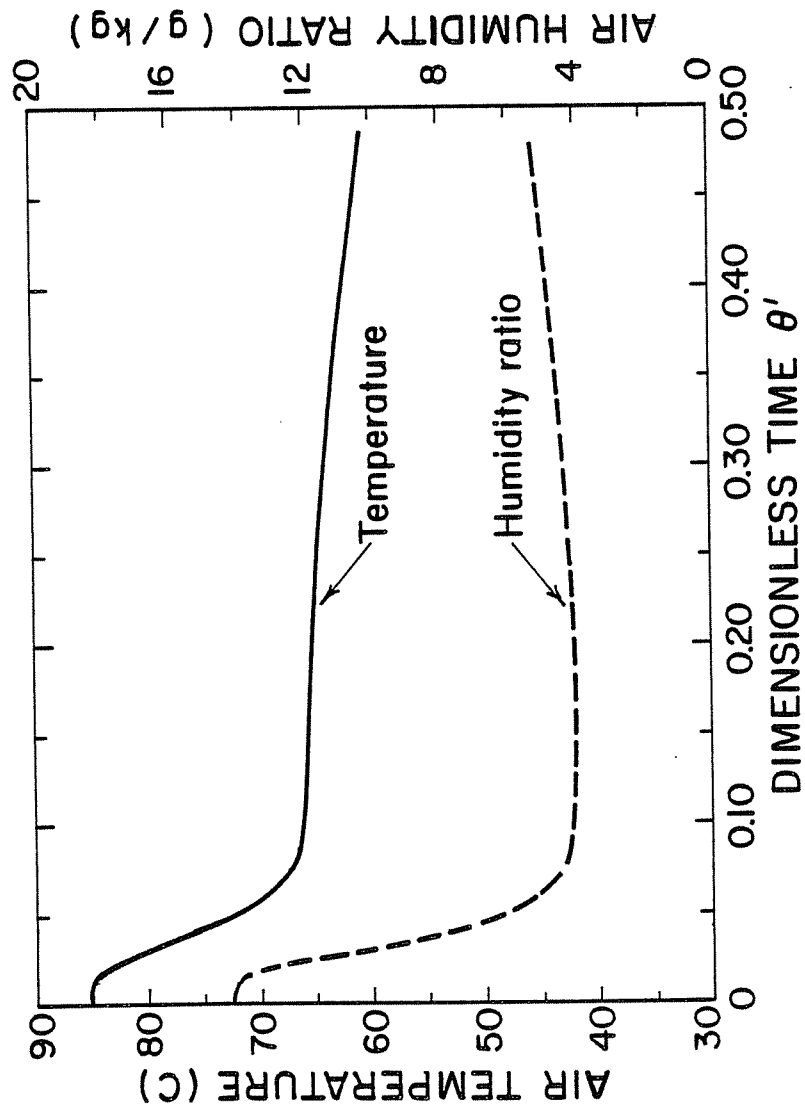


Figure 6.1 Circumferential distribution of the process air stream outlet temperature and humidity

qualitatively show the effect of the recirculated purge stream on the dehumidifier outlet states. The finite difference model of the dehumidifier is then used to determine the outlet and purge states of a counterflow silica gel dehumidifier. In these analyses, the nominal (Table 4.3) silica gel properties are used, and the heat and mass transfer rates are assumed to be limited by convection. Both low and high thermal capacitance matrices are modeled, corresponding to matrices with small and large proportions of non-adsorbing structural materials. The numerical results are used to verify the trends suggested by the equilibrium analysis, and to indicate the improvement in dehumidification and reduction in energy input obtained with the recirculated purge dehumidifier in comparison to a conventional counterflow configuration.

6.1 The Purged Dehumidifier

A schematic diagram of a counterflow dehumidifier with recirculated purge is shown in Figure 6.2. For convenience, a nomenclature similar to that established for the conventional dehumidifier is used, and is illustrated in Figure 6.3. Each period is partitioned into two subperiods, and a particular wheel face is designated $p_{jk,\ell}$. In the recirculation pattern illustrated in Figure 6.2, flow from the outlet of subperiod 1 of period 1 ($p_{11,2}$) is recirculated to the inlet of subperiod 1 in period 2 ($p_{21,1}$). This flow geometry is referred to as the 11 purge or recirculation

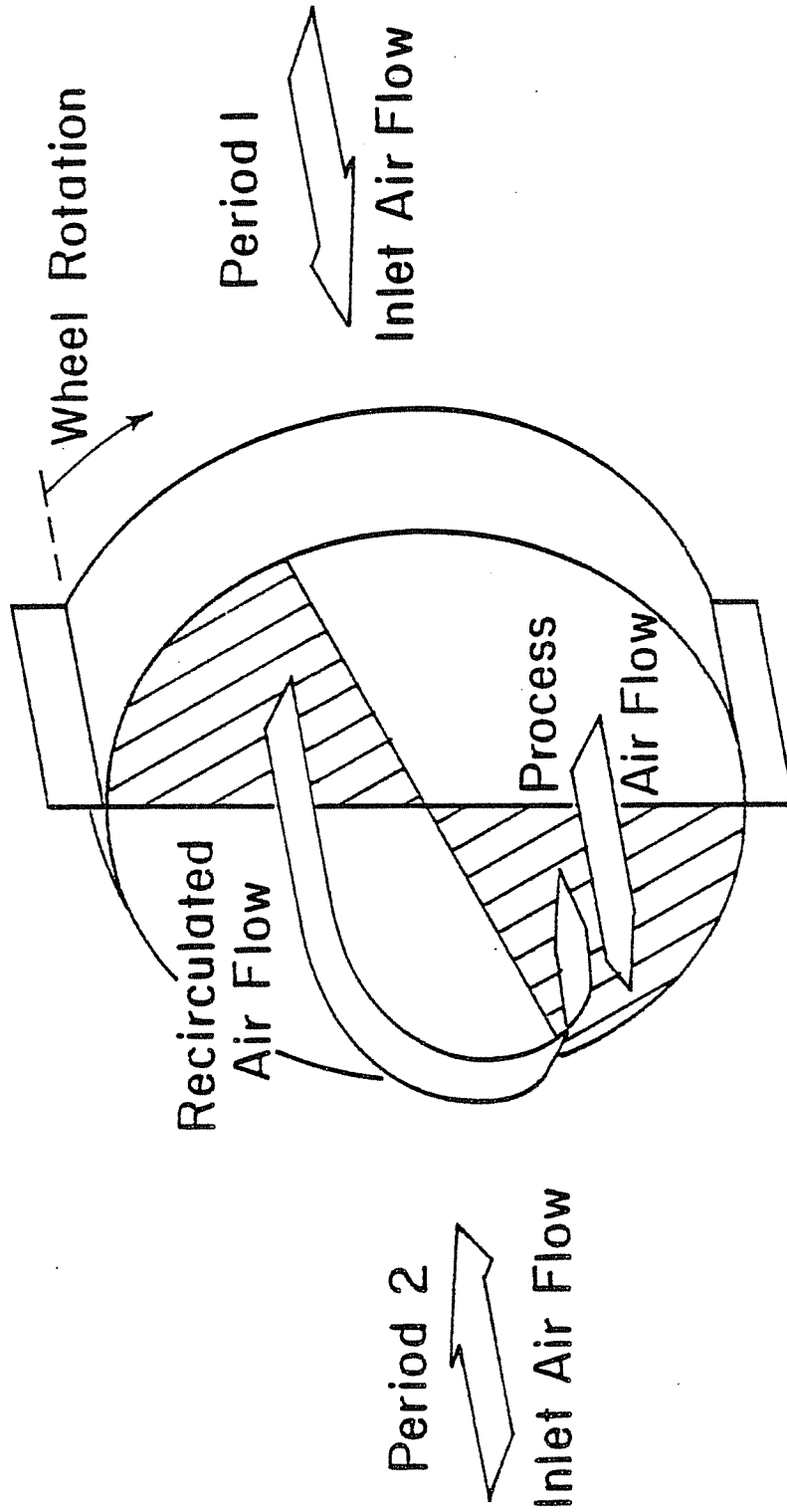


Figure 6.2 Schematic diagram of a counterflow dehumidifier with a recirculated purge stream

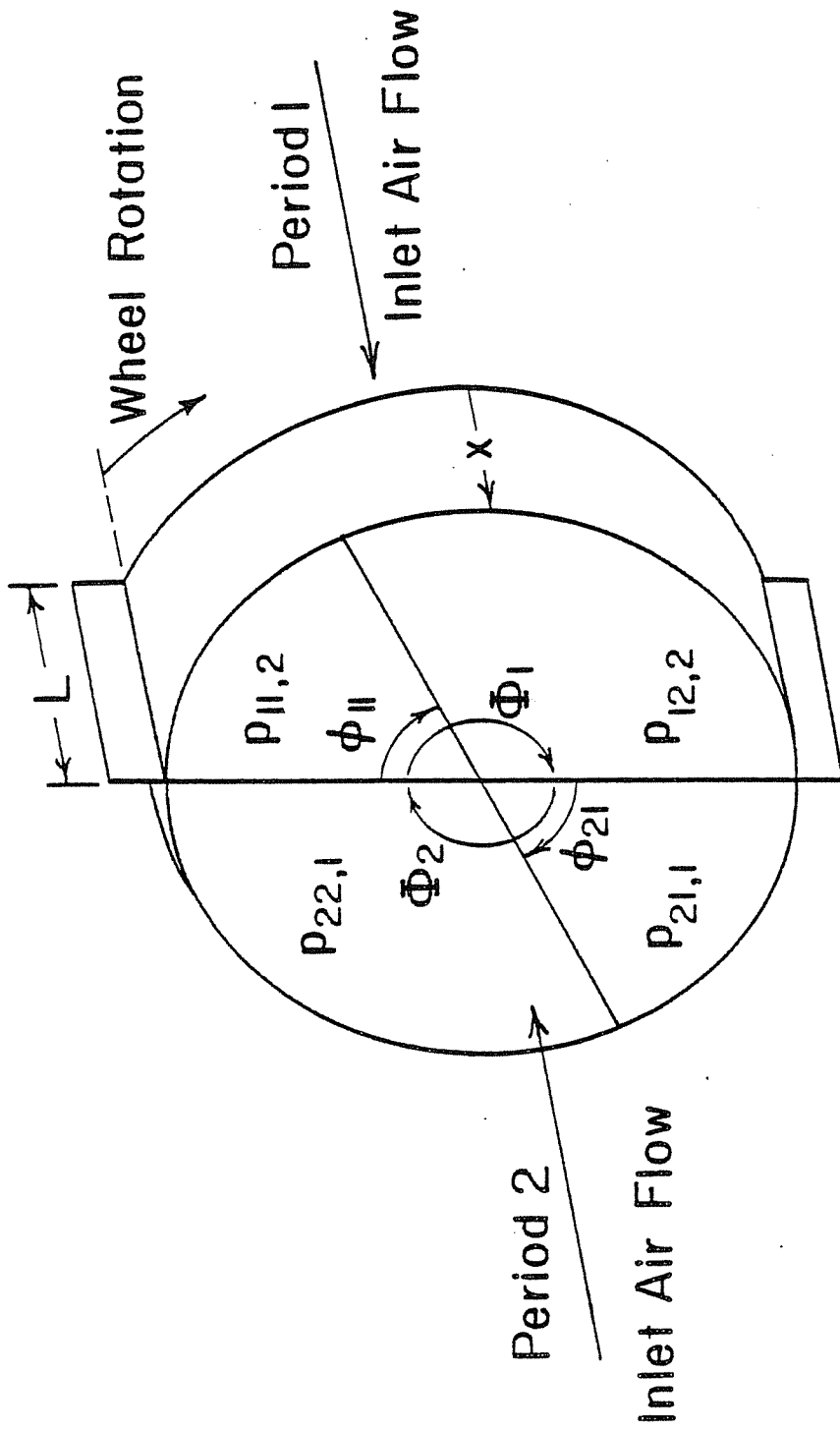


Figure 6.3 Nomenclature for the purged dehumidifier

pattern. The other purge recirculation pattern discussed is from $P_{11,2}$ to $P_{22,1}$, and is referred to as the 12 pattern. The fractional subperiod boundary angle (or time) $\beta_{jk} = \phi_{jk}/\Phi_j$ indicates the size of the purge section. For example, $\beta_{11} = 0.10$ implies that subperiod 1 occupies 10% of the total arc of period 1.

For this system, employing the assumptions stated in §2.2, the conservation equations become

Mass

$$\frac{\partial w}{\partial x'} + \beta_{jk} \theta_j' (\mu_k)_{jk} \frac{\partial W}{\partial \theta'} = 0$$

$j, k=1, 2$ (6.1)

Energy

$$\frac{\partial i}{\partial x'} + \beta_{jk} \theta_j' (\mu_k)_{jk} \frac{\partial I}{\partial \theta'} = 0$$

The transfer rate equations for mass and heat are

Mass

$$\frac{\partial w}{\partial x'} = \Lambda_{jk} (w_m - w_f)$$

$j, k=1, 2$ (6.2)

Energy

$$\frac{\partial i}{\partial x'} = \Lambda_{jk} (Le_o c_f (t_m - t_f) + i_{wv} (w_m - w_f))$$

The recirculation condition is imposed by taking the average purge section outlet temperature and humidity ratio to be the inlet condition for the appropriate subperiod in the regenerating period. The distribution of states in the purged outlet stream is destroyed, but the mean purge state creates a nonuniform inlet condition in the regenerating period. The conservation of mass requires that μK in the two purge subperiods be equal. For example, for the 11 purge shown in Figure 6.2, $\mu K_{11} = \mu K_{21}$.

The finite difference method developed by Maclaine-cross ([18], §2.4.3) was adapted to incorporate the two subperiods in each period. The resulting code is sufficiently flexible to allow the transfer coefficients, air velocities, and inlet states in each subperiod to differ. Both of the rotational time step sizes (§2.4.3) are used in each subperiod, and the mean inlet and outlet states in each subperiod and period are computed. As in the conventional model, the finite difference solution for the dehumidifier outlet states was obtained for three space-time grid sizes, and these results were extrapolated to zero grid sizes. Convergence to periodic steady state at each grid size was established by moisture and energy balances on the air streams. The final extrapolated solution is also checked for moisture and energy conservation.

6.2 Equilibrium Analysis of the Purged Dehumidifier

If the transfer coefficients in Eqs. (6.2) are infinite, then,

in exactly the same manner as for the unpurged dehumidifier, Eqs.

(6.1) may be written as

$$\frac{\partial f_i}{\partial x^i} + \theta_j' \beta_{jk} C_{i,jk} \frac{\partial F_i}{\partial \theta} = 0 \quad \begin{matrix} i=1,2 \\ j=1,2 \end{matrix} \quad (6.3)$$

where $C_{i,jk} = \mu \kappa_{jk} \gamma_i$. Unlike the examples discussed in §3.3, the solution of Eqs. (6.3) requires consideration of the nonuniform regenerating stream inlet state distribution resulting from recirculation of the purged flow. Close [40] and Brandemuehl [46] have extended the equilibrium F_i analysis of rotary dehumidifiers to include arbitrary inlet state distributions. The analysis of the purged dehumidifier is a special case of this general technique.

This discussion will be restricted to a balanced and symmetric dehumidifier with constant γ_i . In addition to being balanced overall, the air velocities, $v_{j,k}$, in all of the subperiods are taken to be equal. Since $v_{m,k}$ and all properties are constant, $C_{i,j} = \beta_{j,k} C_{i,jk}$, and the wave velocities in each subperiod are equal, $V_{i,jk} = V_{i,j} = V_i$. This implies that F_i lines on the wave diagrams do not change slope across subperiod boundaries.

There are two purge geometries to consider, the 11 ($p_{11,2}$ to $p_{21,1}$) recirculation pattern and the 12 ($p_{11,2}$ to $p_{22,1}$) path. For each flow pattern, the purge angle β_{11} can be less than or greater than the rotational arc associated with the F_{1r} wave (i.e., $\beta_{11} \leq C_{1,1}$ or $\beta_{11} > C_{1,1}$). In each case, it is assumed that the purged

air is fully mixed prior to introduction at the inlet of a subperiod in period 2. The F_1 and F_2 wave diagrams for these four cases are illustrated in Figures 6.4-6.7. Figures 6.4 and 6.6 are for $\beta_{11} \leq C_{1,1}$, corresponding to an incomplete purge of the regeneration F_1 state, while Figs. 6.5 and 6.7 illustrate $\beta_{11} > C_{1,1}$ cases. In all of these diagrams, "p" is the process inlet state, "pr" is the purge state, "r" is the regenerating state, and "o" is the process outlet state. Table 6.1 summarizes the wave diagram solutions for the period 1 mean outlet state, the mean purge state, and the process stream outlet state.

Figure 6.4 shows the wave diagrams for the 11 recirculation pattern with $\beta_{11} \leq C_{1,1}$. Since $\beta_{1,1} < C_{1,1} < C_{2,1}$, then $F_{1pr} = F_{1r}$ and $F_{2pr} = F_{2r}$, and the purge state is just the regenerating inlet state. The process outlet state lies on the F_2 line through the regenerating state between the period 1 intersection point and the regenerating inlet state. The mean period 1 outlet state and the distribution of period 1 outlet states are unaffected by the 11 purge recirculation. The 11 purge with $\beta_{11} \leq C_{1,1}$ shifts the process outlet state toward the period 1 intersection point, corresponding to improved dehumidification.

The F_i wave diagrams for the 11 recirculation with $\beta_{11} > C_{1,1}$ are shown in Figure 6.5. Since $C_{1,1} < \beta_{11} < C_{2,1}$, the F_{1pr} is a weighted average of F_{1p} and F_{1r} , while the F_{2pr} is F_{2r} . The purge state lies on the F_2 line through the regenerating inlet state between the period 1 intersection point and the regenerating state.

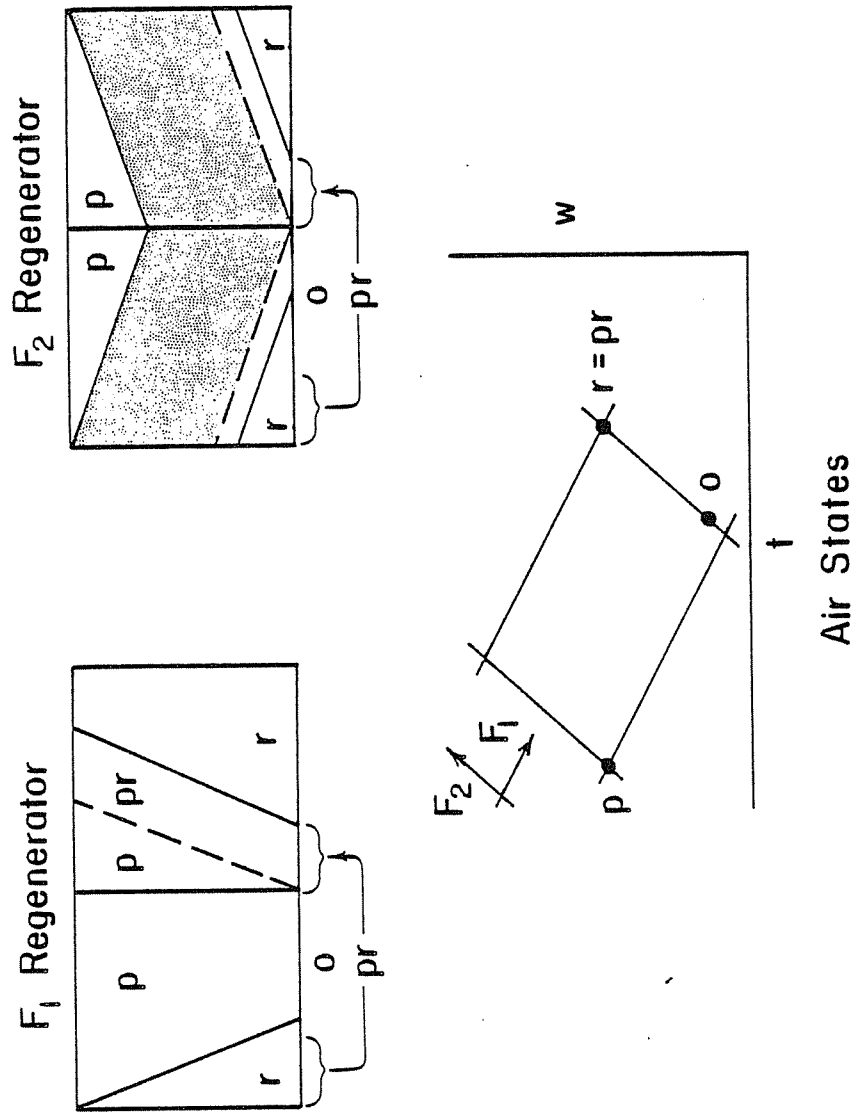


Figure 6.4 F_i wave diagrams for the 11 purge dehumidifier with $\beta_{11} < C_{1,1}$

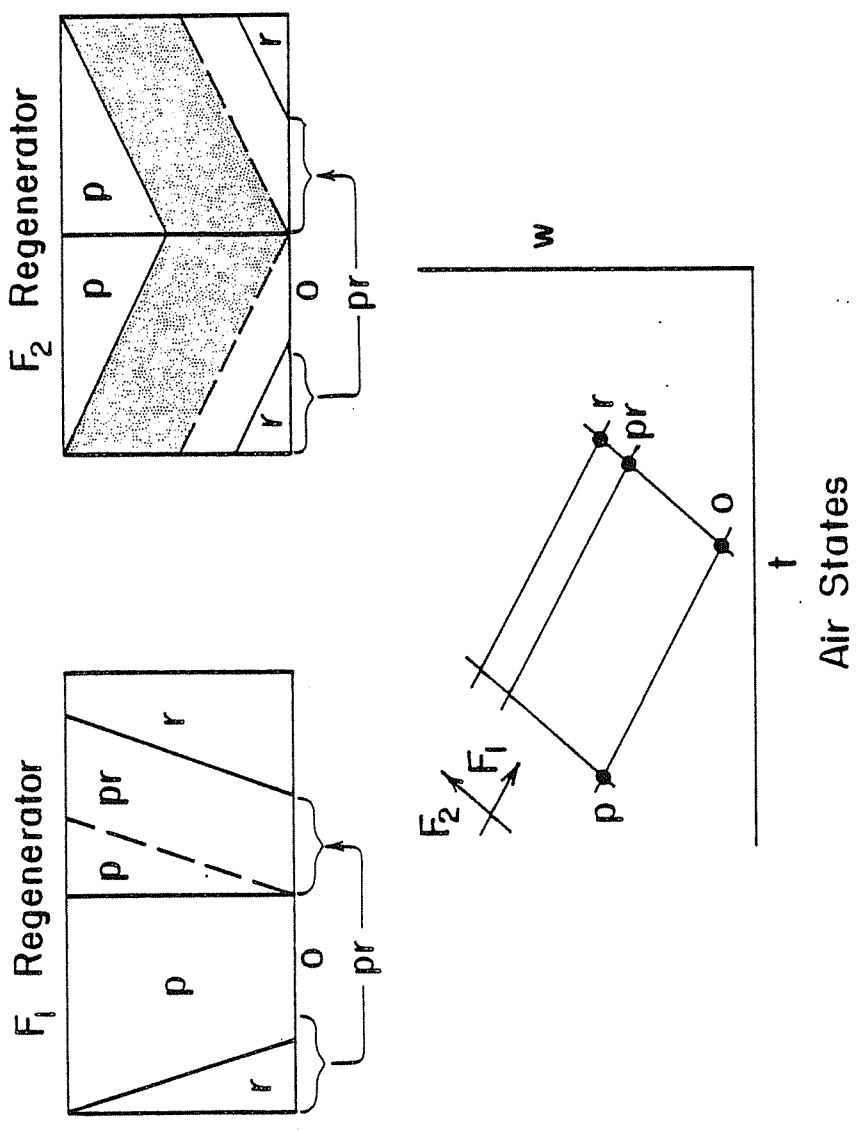


Figure 6.5 F_i wave diagrams for the 11 purge dehumidifier with $\beta_{11} > C_{1,1}$

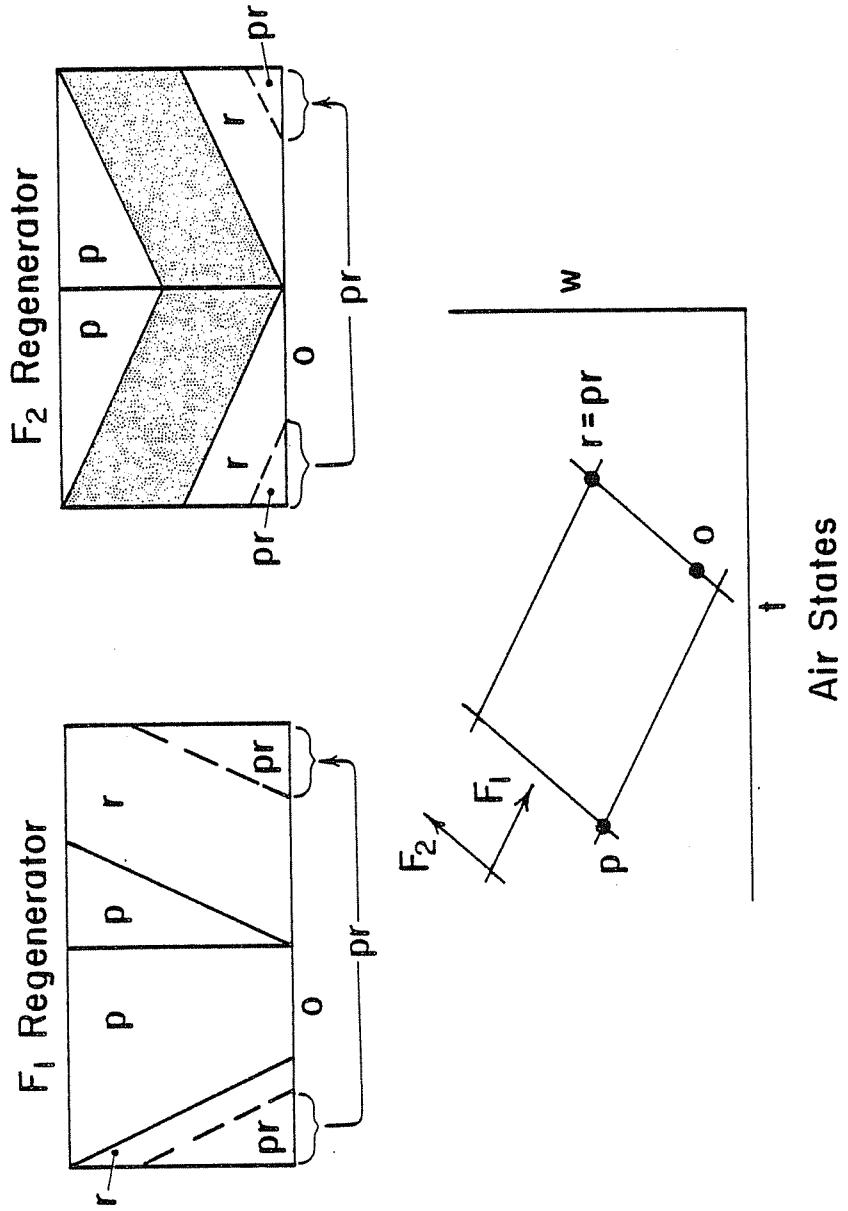


Figure 6.6 F_i wave diagrams for the 12 purge dehumidifier with $\beta_{11} < C_{1,1}$

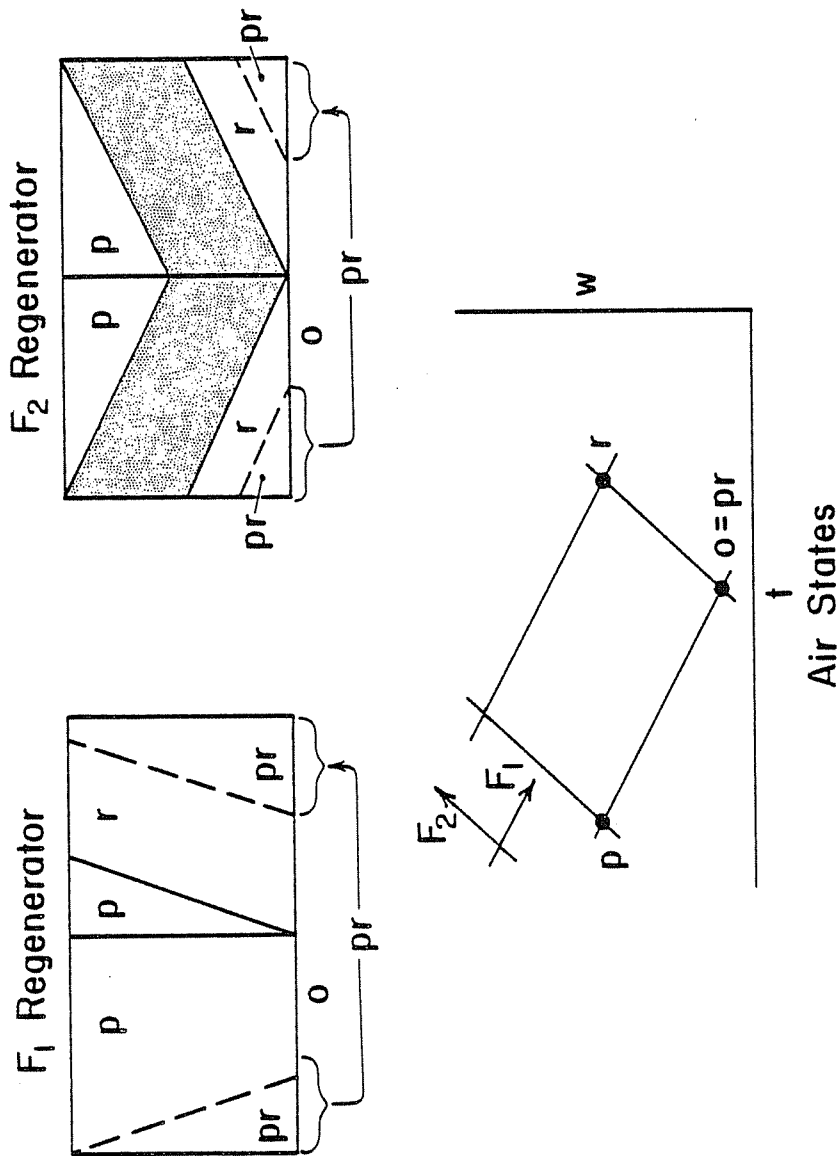


Figure 6.7 F_i wave diagrams for the 12 purge dehumidifier with $\beta_{II} > C_{1,1}$

Table 6.1 Equilibrium solutions for the counterflow purged dehumidifier

p = process inlet ($p_{11,1} = p_{12,1}$) state

r = regenerating inlet ($p_{21,1}$ or $p_{22,1}$) state

x = arbitrary state

	$\beta_{1,1} \leq C_{1,1}$	$\beta_{1,1} > C_{1,1}$
<u>11 recirculation</u>		
period 1 mean	$F_1 \quad C_{1,1}F_{1,r} + (1-C_{1,1})F_{1,p}$	$C_{1,1}F_{1,r} + (1-C_{1,1})F_{1,p}$
	$F_2 \quad F_{2,4}$	$F_{2,4}$
purge($p_{11,2}$)	$F_1 \quad F_{1,r}$	$\frac{C_{1,1}}{\beta_{1,1}}F_{1,r} + (1-\frac{C_{1,1}}{\beta_{1,1}})F_{1,p}$
	$F_2 \quad F_{2,r}$	$F_{2,r}$
process($p_{12,2}$)	$F_1 \quad \frac{C_{1,1}-\beta_{1,1}}{1-\beta_{1,1}}F_{1,r} + \frac{1-C_{1,1}}{1-\beta_{1,1}}F_{1,p}$	$F_{1,p}$
	$F_2 \quad F_{2,r}$	$F_{2,r}$
<u>12 recirculation</u>		
period 1 mean	$F_1 \quad \beta_{1,1}F_{1,x} + (C_{1,1}-\beta_{1,1})F_{1,r} + (1-C_{1,1})F_{1,p}$	$F_{1,p}$
	$F_2 \quad \beta_{1,1}F_{2,x} + (1-\beta_{1,1})F_{2,r}$	$\beta_{1,1}F_{2,x} + (1-\beta_{1,1})F_{2,r}$
purge($p_{11,2}$)	$F_1 \quad F_{1,x}$	$F_{1,p}$
	$F_2 \quad F_{2,x}$	$F_{2,x}$
process($p_{12,2}$)	$F_1 \quad \frac{C_{1,1}-\beta_{1,1}}{1-\beta_{1,1}}F_{1,r} + \frac{1-C_{1,1}}{1-\beta_{1,1}}F_{1,p}$	$F_{1,p}$
	$F_2 \quad F_{2,r}$	$F_{2,r}$

The process outlet state is at the intersection point of the F_{1p} and F_{2r} lines. The distribution and mean of the period 1 outlet states are identical to those for the 11 purge with $\beta_{11} \leq C_{1,1}$.

The solution for the 12 recirculation pattern with $\beta_{11} \leq C_{1,1}$ is shown in Figure 6.6. The F_i diagrams indicate that for balanced flow with constant γ_i , the purge states are recycled through the matrix, and the F_{ipr} are completely arbitrary. The process outlet state F_i are identical to those for the 11 purge with $\beta_{11} \leq C_{1,1}$. Since the purge state is arbitrary, the period 1 outlet state distribution is arbitrary for $\theta' < \beta_{11}\theta'_1$, and the period 1 mean is also arbitrary. In a system with variable γ_i or finite transfer coefficients, the wave fronts smear and the purge state, rather than being arbitrary as in the constant γ_i equilibrium case, would tend to the regenerating state. In this case, the 12 recirculation with $\beta_{11} \leq C_{1,1}$ would result in the same dehumidifier outlet states as the 11 recirculation with $\beta_{11} \leq C_{1,1}$.

The 12 purge with $\beta_{11} > C_{1,1}$ is illustrated in Figure 6.7. As in the previous case, the F_{2pr} state is completely arbitrary. However, F_{1pr} is given by

$$F_{1pr} = \frac{C_{1,1}}{\beta_{11}} F_{1pr} + \left(1 - \frac{C_{1,1}}{\beta_{11}}\right) F_{1p} \quad (6.4)$$

which is satisfied only for $F_{1pr} = F_{1p}$. The matrix is uniformly at F_{1p} during period 1. The purge state lies anywhere along the F_{1p} line. The process outlet state is at the period 1 intersection

point, as it is for the 11 purge with $\beta_{11} > C_{1,1}$. Since F_{2pr} is recycled through the matrix, the period 1 F_2 distribution is arbitrary for $\theta' < \beta_{11}\theta'_1$, and the period 1 mean state lies somewhere on the F_{1p} line. If the wave fronts smear, then $F_{2pr} = F_{2r}$. In this case, the period 1 outlet is uniformly at the intersection point of the F_{1p} and F_{2r} characteristics, and the period mean, purge, and process outlet states are all equal.

The equilibrium analysis of the balanced flow, constant γ_i recirculated purge dehumidifier indicates that the distribution of states in the matrix, and hence the purge and mean period 1 states can be influenced by the recirculation geometry. However, the process outlet state ($p_{12,2}$) depends only on the magnitude of β_{11} in relation to $C_{1,1}$ and is unaffected by the recirculation geometry. As β_{11} increases, the fraction of the flow through period 1 of the dehumidifier that goes to the process decreases as does the required regenerating flow. At $\beta_{11} = C_{1,1}$, just the regenerating state F_1 is purged, and the minimum outlet humidity ratio is obtained. For $\beta_{11} > C_{1,1}$, there is no change in process outlet state, but the useful process flow rate is decreased. This suggests that the optimum purge angle, regardless of the recirculation pattern, is $\beta_{11} = C_{1,1}$.

6.3 Numerical Analysis of the Purged Dehumidifier

The finite difference solution was used to determine the effect

of purge angle β_{11} on the period 1 outlet states of a counterflow silica gel dehumidifier. The dehumidifier is taken to be symmetric ($\theta_1' = \theta_2' = 0.50$) and balanced overall ($\mu\kappa_1 = \mu\kappa_2 = \mu\kappa$) with equal subperiod velocities. The overall Lewis number is assumed to be unity. Results are presented for two silica gel matrices, one with negligible matrix structural thermal capacitance, the other with appreciable thermal capacitance of non-adsorbing structure. In the former case, the bulk thermal capacitance of silica gel is used ($c_m = 921 \text{ J/(kg-}^\circ\text{C)}$); in the latter, the value corresponding to a matrix that is 50% mylar or 44% aluminum by volume is employed ($c_m = 3350 \text{ J/(kg-}^\circ\text{C)}$). The solution for a $\Lambda_{jk} = 20.0$ ($\text{NTU}_o = 10$) dehumidifier is determined for the two pairs of inlet states used in 3.5. Inlet state pair 1 is (35°C , 14.2 g/kg) and (85°C , 14.2 g/kg) and inlet state pair 2 is (26.7°C , 11.1 g/kg) and (85°C , 18.8 g/kg). The rotational speeds considered are $\mu\kappa = 0.20$ for the bulk silica gel dehumidifier, and $\mu\kappa = 0.125$ for the high thermal capacity matrix. These $\mu\kappa$ are nearly optimal for the silica gel dehumidifier (§3.5.1 and §4.4.6).

The finite difference solution was used to verify the qualitative trends in purged dehumidifier performance predicted by the equilibrium analysis. Figures 6.8 and 6.9 illustrate the period 1 outlet air temperature and humidity ratio distributions for the 11 and 12 recirculation patterns for $\beta_{11} = 0.025$, 0.0875 , and 0.150 for a low thermal capacitance dehumidifier with inlet state pair 1 and $\mu\kappa = 0.20$. For this case, $C_{1,1} \approx 0.0875$, so that the selected

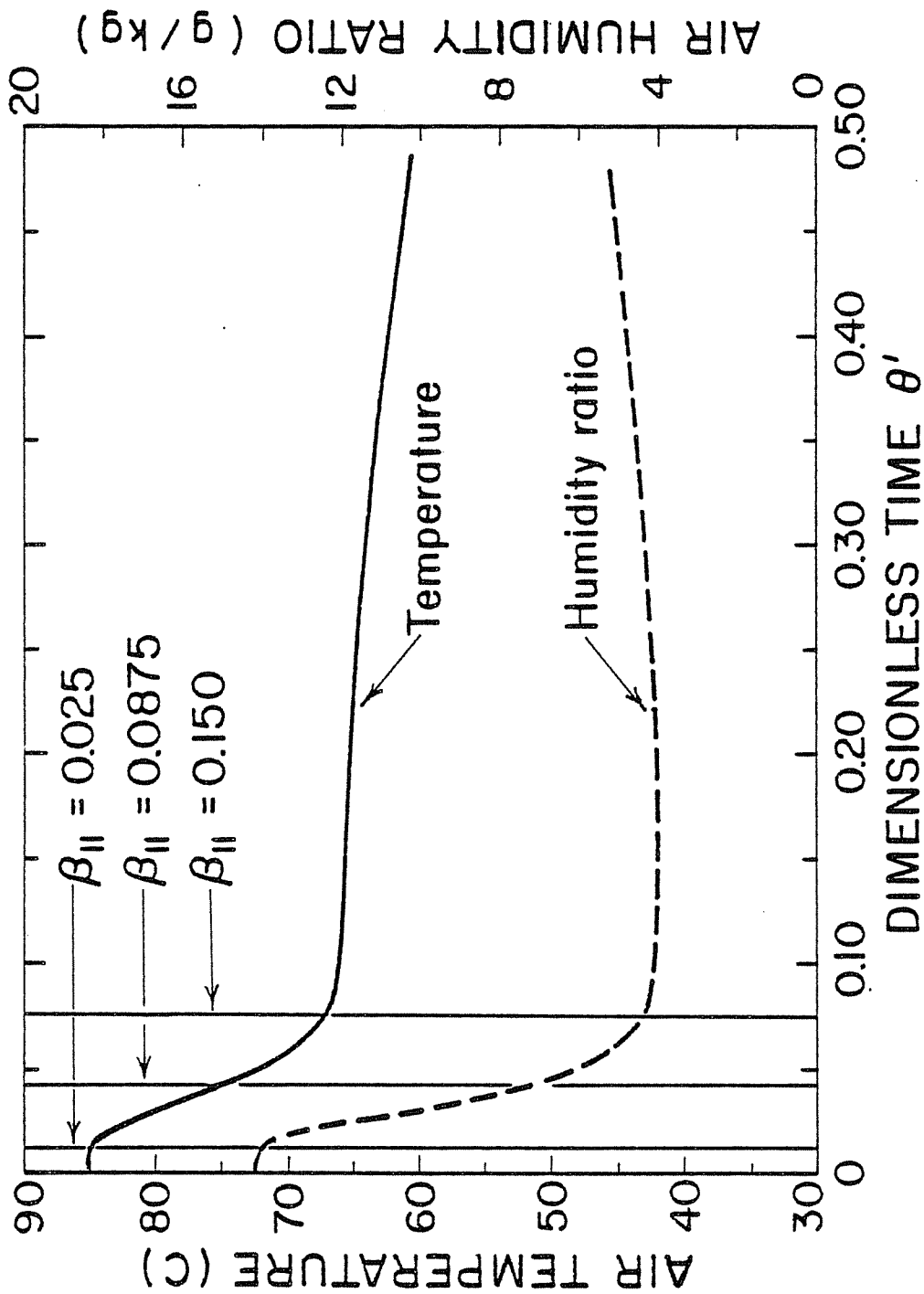


Figure 6.8 Process stream outlet state distributions for the 11 purge dehumidifier with $\beta_{11} = 0.025, 0.0875, \text{ and } 0.150$

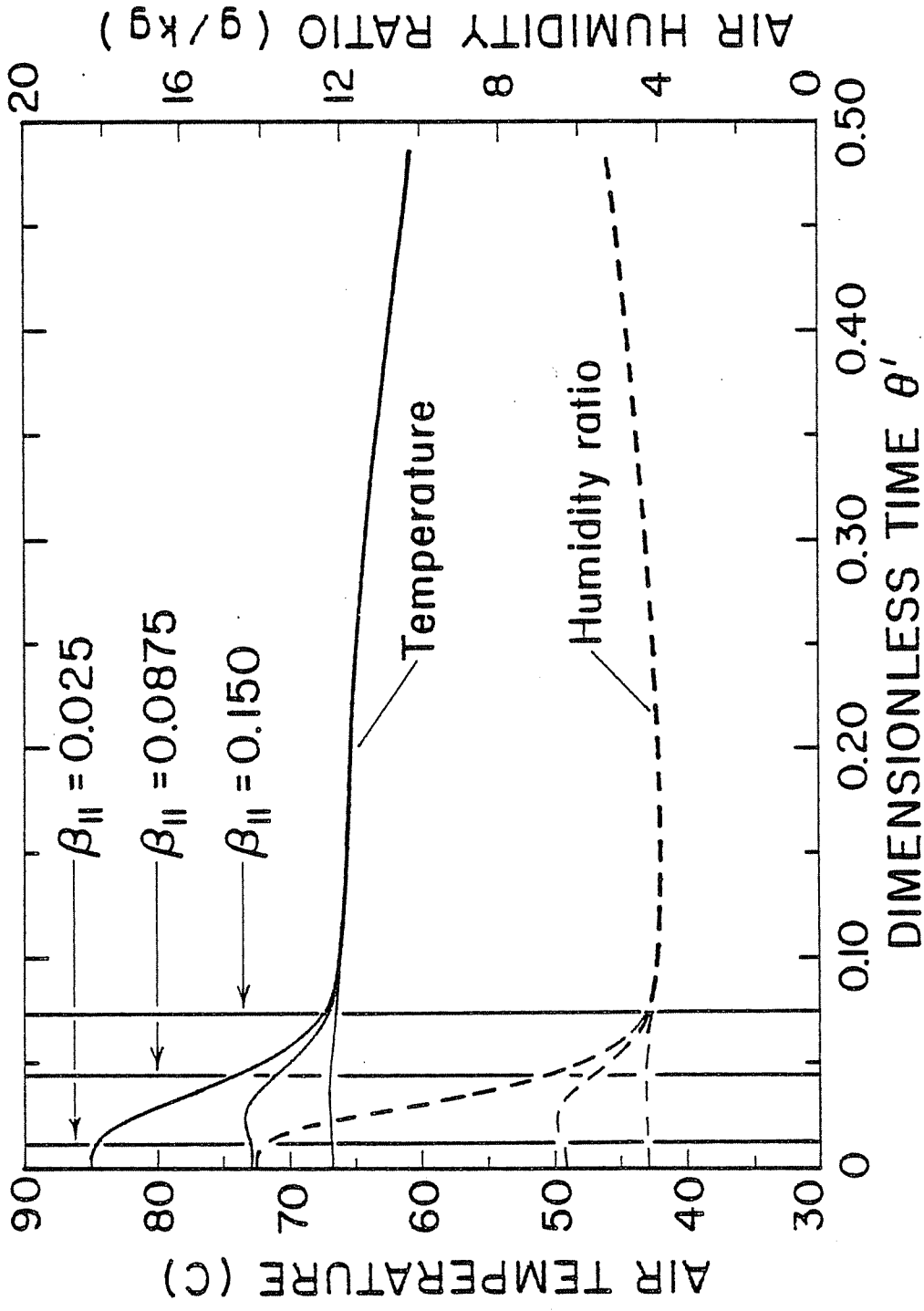


Figure 6.9 Process stream outlet state distributions for the 12 purge dehumidifier with $\beta_{II} = 0.025, 0.0875, \text{ and } 0.150$

range of β_{11} spans the two modes of purge operation discussed in 6.2. Table 6.2 gives the period 1 mean outlet state, the mean purge state, and the mean process outlet state for the cases considered.

The equilibrium solution in Table 6.1 indicate that β_{11} does not affect the period 1 outlet state distributions for the 11 purge geometry. This result is substantiated by the period 1 outlet temperature and humidity ratio distributions shown in Figure 6.8 and the mean period 1 outlet states listed in Table 6.2 for the 11 purge. From Table 6.2 it can be seen that the variation with β_{11} of the average period 1 outlet temperature and humidity ratio is 0.1°C and 0.02 g/kg , much less than 1% of the total change in period 1 air state from the inlet conditions. Since the γ_i are not constant and the transfer coefficients are finite, the outlet distributions are not discontinuous at $\theta' = C_{1,1}\theta_1'$ but change smoothly about $\theta' = C_{1,1}\theta_1'$ from the regenerating state to a state approximately equal to the F_1 intersection point. The change in the 11 purge state indicated in Table 6.2 is due to incorporation of the transition region around $\theta' = C_{1,1}\theta_1'$ in the purge state rather than because of a substantial change in the outlet distributions. The equilibrium analysis predicts that a minimum in process outlet humidity ratio should be obtained at $\beta_{11} = C_{1,1}$. The numerical results in Table 6.2 show that while the process outlet humidity ratio decreases with increasing β_{11} , the minimum does not occur at $C_{1,1}$ as predicted by the analogy method. Again, this is due to the fact that the outlet

state humidity ratio distribution is not constant for $\theta' > C_{1,1}\theta'$, as occurs in the constant γ_i equilibrium analysis.

The equilibrium solution for the 12 purge dehumidifier was used to argue that finite transfer coefficients and variable γ_i would cause the period 1 outlet state distributions for a 12 purge with $\beta_{11} < C_{1,1}$ to be the same as those for the 11 purge, but for the 12 purge with $\beta_{1,1} > C_{1,1}$, the period 1 temperature and humidity ratio would be constant with θ' . These trends are exhibited by the data shown in Figure 6.9 and Table 6.2 for the 12 purge dehumidifier. For $\beta_{11} = 0.025 < C_{1,1}$, the 11 and 12 outlet state distributions closely resemble each other, and there is only a very small difference between the mean states listed in Table 6.2. For $\beta_{11} = 0.15 > C_{1,1}$, there is considerable difference between the 11 and 12 distributions shown in Figures 6.8 and 6.9. Figure 6.9 shows that the 12 purge period 1 outlet temperature and humidity ratio are nearly constant, as also is indicated by the averages given in Table 6.2. Both the purge state and the process outlet state are close to the period 1 intersection point, as predicted by the equilibrium analysis. The $\beta_{11} = 0.0875 \doteq C_{1,1}$ results show intermediate behavior because of the continuous nature of the outlet state distributions.

These comparisons establish the qualitative utility of the equilibrium analysis using the analogy method.

The mean process outlet states listed in Table 6.2 show that the outlet humidity ratio decreases with increasing β_{11} , which

suggests that there is a purge angle which maximizes the dehumidification of the process air stream. However, there are two measures of the performance of the purged dehumidifier. A performance comparison can be made on the basis of either constant total period flow through the dehumidifier or constant process stream flow rate as the purge fraction is changed.

If the air flow rate to the process is kept constant as β_{11} is increased, then the total flow through the dehumidifier must increase as $(1 - \beta_{11})^{-1}$. The wheel radius must increase as $(1 - \beta_{11})^{-\frac{1}{2}}$ to keep $\mu\kappa$ and Λ constant. The dehumidification per unit process stream flow rate is just the difference between the period 1 inlet and process stream outlet humidity ratios, $w_{1,1} - w_{12,2}$. The purged dehumidifier humidity efficiency is

$$\eta_{wp} = \frac{w_{1,1} - w_{12,2}}{w_{1,1} - w_{1,int}} \quad (6.5)$$

where $w_{i,int}$ is the humidity ratio at the intersection point of the F_1 line through the process period inlet state and the F_2 line through the regenerating inlet state. This is a suitable measure of dehumidifier performance provided that the dehumidifier size and the power to pump air through the dehumidifier are unimportant.

If the total air flow through period 1 is kept constant as β_{11} is increased, then the dehumidified air flow rate decreases as $1 - \beta_{11}$. The dehumidification of the process stream per unit total period 1 flow is $(1 - \beta_{11}) \cdot (w_{1,1} - w_{12,2})$. The effective dehumid-

ification efficiency per unit total process period flow is

$$\eta_{wp}^* = (1 - \beta_{11}) \eta_{wp} = (1 - \beta_{11}) \frac{w_{1,1} - w_{12,2}}{w_{1,1} - w_{1,int}} \quad (6.6)$$

This figure of merit is appropriate if the dehumidifier is of specified diameter or if the power requirement to pump air through the matrix is important.

The effect of β_{11} on the process outlet states of the dehumidifier with inlet state pair 1 is shown by the data in Table 6.3 for the low thermal capacitance matrix and Table 6.4 for the high thermal capacitance matrix. The corresponding normalized dehumidification per unit process stream flow rate, η_{wp} , and dehumidification per total period flow rate, η_{wp}^* , are illustrated in Figure 6.10.

For the low thermal capacitance matrix the 12 recirculation pattern results in a slightly drier process stream outlet state than does the 11 purge. Both purge geometries have a minimum in $w_{12,2}$ at $\beta_{11} \approx 0.125$, which is greater than the optimum $\beta_{11} = C_{1,1} \approx 0.0875$ predicted by the equilibrium analogy analysis. The resulting maximum in η_{wp} is about 7% greater than obtained at $\beta_{11} = 0$. However, as shown in Figure 6.10, η_{wp}^* decreases monotonically with increasing β_{11} . For inlet state pair 1, at fixed total flow through the matrix, the process stream flow rate decreases more rapidly with β_{11} than does the outlet humidity ratio, resulting in a net decrease in useful dehumidification.

Table 6.3 Period 1 outlet states for a low thermal capacitance matrix with inlet state pair 1

process inlet state: (35°C, 14.2 g/kg) : A_{jk} = 20.0
 regenerating inlet state: (85°C, 14.2 g/kg) : μ_{kj} = 0.20
 period 1 intersection point (65.51°C, 3.846 g/kg) : Le₀ = 1

β ₁₁	period 1 mean			purge			process		
	t _{1,2} (°C)	w _{1,2} ($\frac{g}{kg}$)	t _{11,2} (°C)	w _{11,2} ($\frac{g}{kg}$)	t _{12,2} (°C)	w _{12,2} ($\frac{g}{kg}$)			
<u>11 purge</u>	0.0	5.167	-	-	65.96	5.167			
	0.025	5.167	84.96	14.164	65.46	4.937			
	0.050	5.167	84.24	13.540	64.98	4.727			
	0.075	5.169	82.53	12.246	64.58	4.595			
	0.100	5.173	80.45	10.923	64.29	4.534			
	0.125	5.179	78.46	9.817	64.09	4.517			
	0.150	5.187	76.73	8.945	63.93	4.524			
	0.175	5.196	75.31	8.269	63.79	4.544			
	0.200	5.205	74.17	7.745	63.66	4.570			
<u>12 purge</u>	0.0	5.167	-	-	65.96	5.167			
	0.025	5.164	84.85	14.064	65.46	4.936			
	0.050	5.039	81.63	11.375	64.95	4.705			
	0.075	4.791	75.65	7.675	64.51	4.557			
	0.100	4.610	70.79	5.578	64.22	4.563			
	0.125	4.515	67.94	4.625	64.04	4.499			
	0.150	4.478	66.71	4.271	63.92	4.515			
	0.175	4.472	66.31	4.163	63.80	4.537			
	0.200	4.476	66.16	4.128	63.69	4.563			

Table 6.4 Period 1 outlet states for a high thermal capacitance matrix with inlet state pair 1

process inlet state: (35°C, 14.2 g/kg) ; ; $\Delta jk = 20.0$
 regenerating inlet state: (85°C, 14.2 g/kg) ; ; $\mu kj = 0.125$
 period 1 intersection point: (74.76°C, 3.959 g/kg) ; ; $Le_0 = 1.0$

	period 1 mean			purge			process		
	β_{11}	$t_{1,1}$ (°C)	$w_{1,2}$ ($\frac{g}{kg}$)	$t_{11,2}$ (°C)	$w_{11,2}$ ($\frac{g}{kg}$)	$t_{12,2}$ (°C)	$w_{12,2}$ ($\frac{g}{kg}$)		
<u>11 purge</u>	0.0	70.17	6.472	-	-	70.17	6.472		
	0.025	70.17	6.472	85.00	14.196	69.78	6.274		
	0.050	70.17	6.472	84.92	14.079	69.38	6.072		
	0.075	70.17	6.472	84.59	13.590	68.98	5.895		
	0.100	70.17	6.472	84.02	12.802	68.61	5.769		
	0.125	70.17	6.472	83.33	11.937	68.27	5.692		
	0.150	70.16	6.473	82.61	11.124	67.94	5.652		
	0.175	70.15	6.474	81.93	10.407	67.63	5.640		
	0.200	70.14	6.476	81.29	9.793	67.33	5.647		
<u>12 purge</u>	0.0	70.17	6.472	-	-	70.17	6.472		
	0.025	70.17	6.472	84.99	14.188	69.78	6.274		
	0.050	70.15	6.446	84.66	13.672	69.38	6.066		
	0.075	70.03	6.291	83.17	11.534	68.96	5.866		
	0.100	69.83	6.056	81.11	9.067	68.57	5.722		
	0.125	69.61	5.854	79.31	7.320	68.22	5.644		
	0.150	69.42	5.710	77.98	6.248	67.90	5.615		
	0.175	69.27	5.618	77.09	5.636	67.61	5.614		
	0.200	69.16	5.566	76.49	5.307	67.33	5.630		

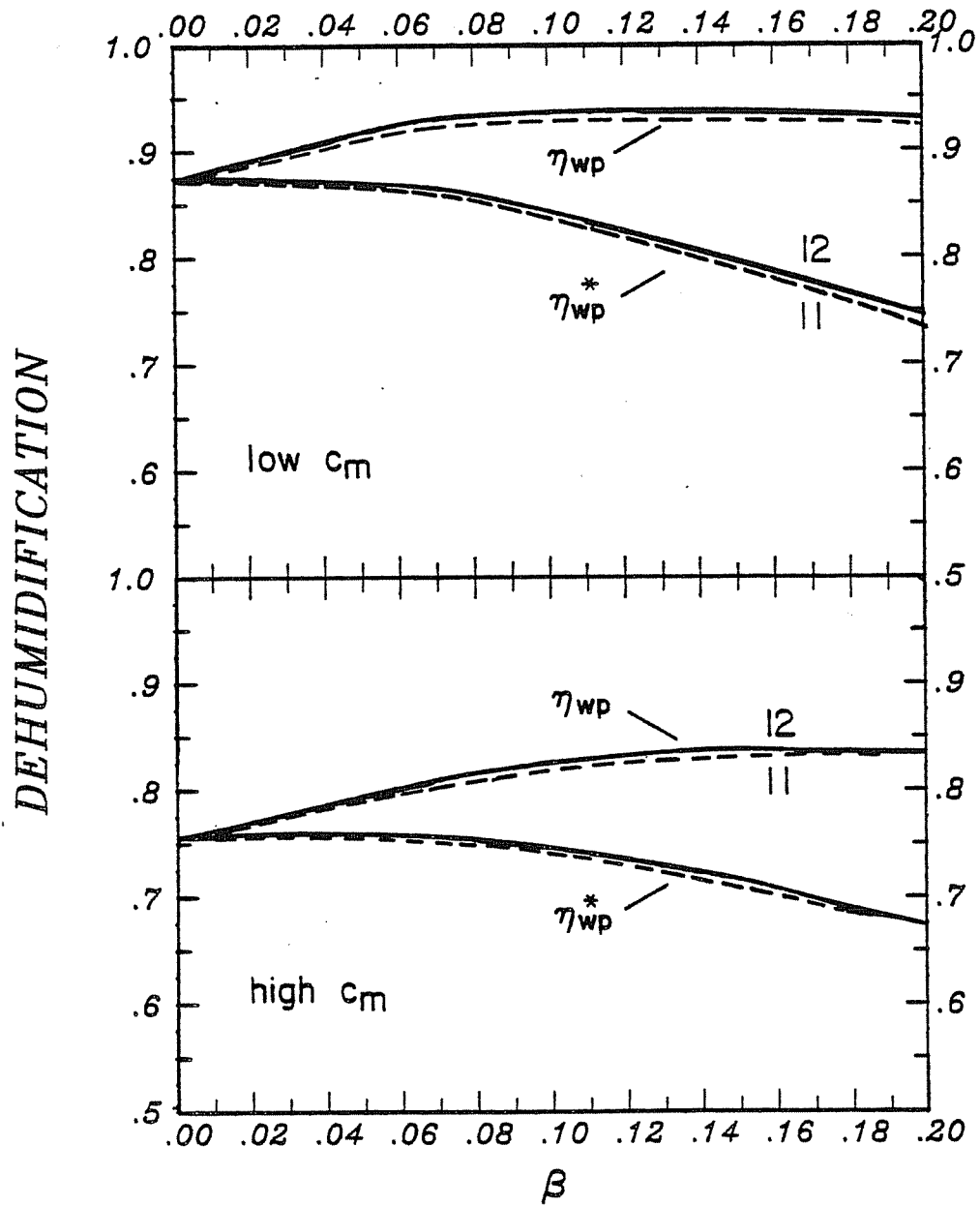


Figure 6.10 η_{wp} and η_{wp}^* for a low and high thermal capacitance purged dehumidifiers with inlet state pair 1

The effect of β_{11} on a high thermal capacitance dehumidifier with inlet state pair 1 is given by data in Table 6.4 and Figure 6.10. The process stream outlet states are about 4°C hotter and 1.3 g/kg wetter than those for the low capacitance dehumidifier. The 12 recirculation again results in slightly greater dehumidification of the process stream than does the 11 purge. The optimum purge angle is larger than for the low capacitance dehumidifier, at $\beta_{11} = 0.175$. The optimum purge angle observed for the high capacitance dehumidifier is greater than the optimum angle of 0.105 predicted by the equilibrium method. The maximum dehumidification per unit process flow rate, η_{wp} , is about 11% greater than was obtained at $\beta_{11} = 0.0$, which is a larger increase than was obtained for the low thermal capacitance dehumidifier. However, as was the case for the low thermal capacitance dehumidifier, Figure 6.10 shows that the dehumidification per unit total period flow rate, η_{wp}^* , decreases with increasing β_{11} for inlet state pair 1. Although purging has a greater beneficial effect on the performance of the high thermal capacitance dehumidifier than for the low capacitance dehumidifier, the low thermal capacitance matrix results in greater dehumidification than can be obtained using the high thermal capacitance matrix.

The corresponding results for inlet state pair 2 are given in Tables 6.5 and 6.6 and Figure 6.11. As was observed for inlet state pair 1, for both dehumidifiers, the 12 recirculation results in slightly greater dehumidification of the process stream than does

Table 6.5 Period 1 outlet states for a low thermal capacitance matrix with inlet state pair 2

process inlet state: (26.7°C, 11.1 g/kg) : $\Delta_{jk} = 20$
 regenerating inlet state: (85°C, 18.8 g/kg) : $\mu_{kj} = 0.20$
 period 1 intersection point: (52.16°C, 2.151 g/kg) : $Le_0 = 1.0$

β_{11}	period 1 mean			purge			process		
	$t_{1,2}$ (°C)	$w_{1,2}$ ($\frac{g}{kg}$)	$t_{11,2}$ (°C)	$w_{11,2}$ ($\frac{g}{kg}$)	$t_{12,2}$ (°C)	$w_{12,2}$ ($\frac{g}{kg}$)	$t_{12,2}$ (°C)	$w_{12,2}$ ($\frac{g}{kg}$)	
<u>11 purge</u>	0.0	55.55	3.517	-	-	55.55	3.517		
	0.025	55.72	3.534	84.90	18.676	54.95	3.145		
	0.050	55.62	3.525	83.57	17.262	54.11	2.802		
	0.075	55.56	3.519	81.02	15.030	53.45	2.586		
	0.100	55.52	3.518	78.05	12.970	52.97	2.468		
	0.125	55.48	3.520	75.10	11.303	52.64	2.408		
	0.150	55.44	3.525	72.37	9.993	52.42	2.383		
	0.175	55.40	3.532	69.95	8.963	52.28	2.380		
	0.200	55.36	3.540	67.88	8.147	52.20	2.388		
<u>12 purge</u>	0.0	55.55	3.517	-	-	55.55	3.517		
	0.025	55.70	3.521	84.58	18.300	54.94	3.142		
	0.050	55.32	3.266	78.93	12.770	54.05	2.765		
	0.075	54.68	2.931	71.19	7.771	53.32	2.538		
	0.100	53.99	2.695	64.63	5.095	52.81	2.429		
	0.125	53.36	2.545	59.57	3.681	52.47	2.382		
	0.150	52.86	2.456	56.16	2.954	52.28	2.369		
	0.175	52.54	2.411	54.25	2.610	52.18	2.369		
	0.200	52.36	2.392	53.38	2.467	52.11	2.374		

Table 6.6 Period 1 outlet states for a high thermal capacitance matrix with inlet state pair 2

process inlet state (26.7°C, 11.1 g/kg) : Δjk = 20.0
 regenerating inlet state (85°C, 18.8 g/kg) : μkj = 0.125
 period 1 intersection point (61.49°C, 1.219 g/kg) : Le₀ = 1.0

β ₁₁	period 1 mean			purge			process																																							
	t _{1,1} (°C)	w _{1,2} ($\frac{g}{kg}$)	t _{11,2} (°C)	w _{11,2} ($\frac{g}{kg}$)	t _{12,2} (°C)	w _{12,2} ($\frac{g}{kg}$)																																								
<u>11 purge</u>	0.0	4.217	-	-	62.59	4.217	0.025	4.241	84.99	62.10	3.868	0.050	4.236	84.78	61.47	3.491	0.075	4.231	84.12	60.86	3.174	0.100	4.226	83.12	60.30	2.943	0.125	4.223	81.99	59.79	2.784	0.150	4.222	80.83	59.31	2.676	0.175	4.222	79.71	58.86	2.603	0.200	4.224	78.63	58.44	2.558
<u>12 purge</u>	0.0	4.217	-	-	62.59	4.217	0.025	4.240	84.97	62.10	3.868	0.050	4.152	84.03	61.45	3.473	0.075	3.840	81.29	60.80	3.115	0.100	3.490	78.21	60.20	2.858	0.125	3.203	75.48	59.65	2.690	0.150	2.981	73.13	59.16	2.582	0.175	2.810	71.08	58.72	2.515	0.200	2.679	69.29	58.31	2.478

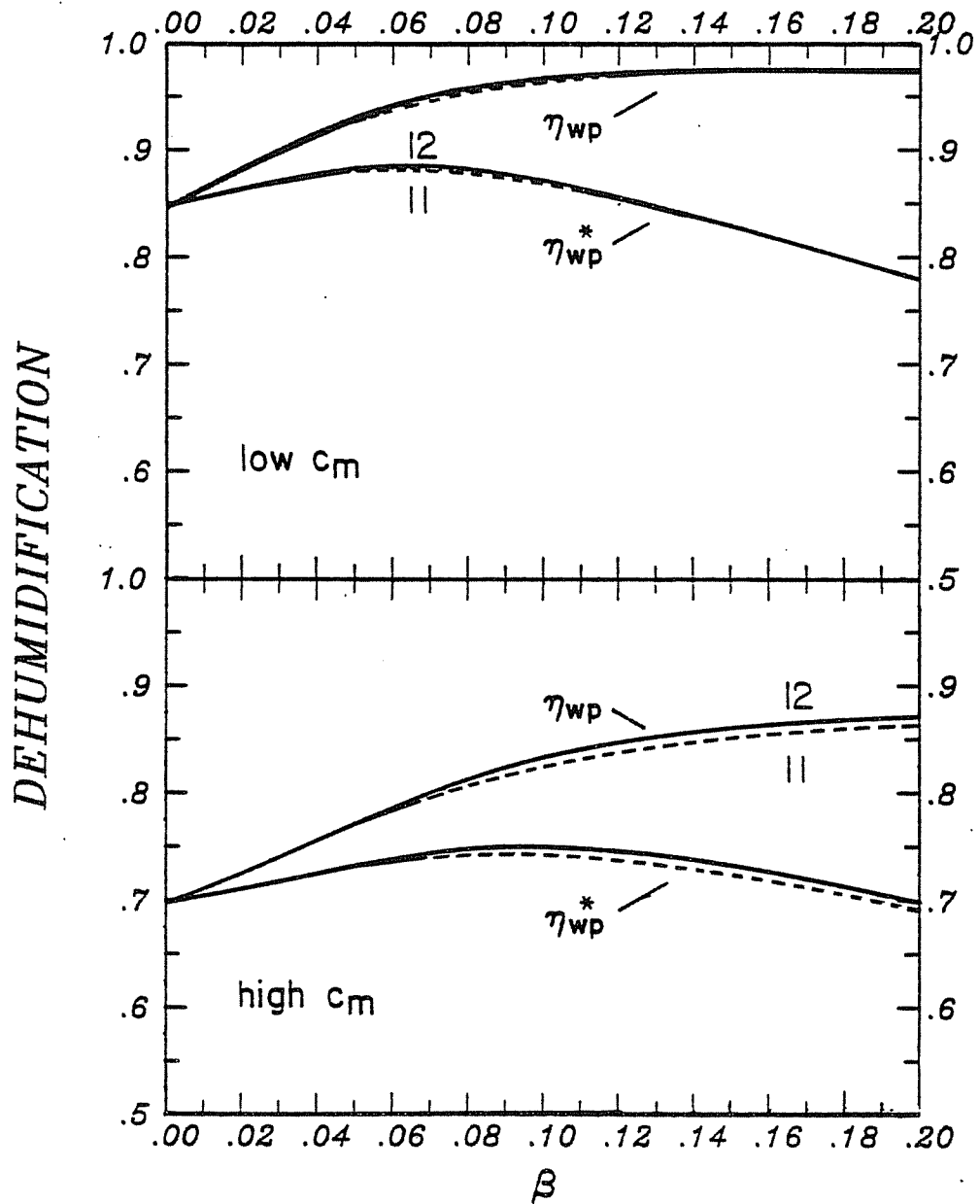


Figure 6.11 η_{wp} and η_{wp}^* for the low and high thermal capacitance purged dehumidifiers with inlet state pair 2

the 11 purge. For the low thermal capacitance matrix, the minimum $w_{12,2}$ occurs at $\beta_{11} = 0.175$, which is greater than the optimum purge angle for inlet state pair 1, and nearly twice the optimum value of $\beta_{11} = C_{1,1} \approx 0.094$ predicted by the equilibrium analysis. The resulting maximum in process stream dehumidification is almost 15% greater than was obtained with $\beta_{11} = 0.0$. Also, from Figure 6.12 it can be seen that for the low capacitance dehumidifier at $\beta_{11} = 0.06$ there is a maximum in η_{wp}^* the dehumidification per unit total period flow, that is about 4% greater than the $\beta_{11} = 0.0$ value.

Similar data for the high thermal capacitance dehumidifier with inlet state pair 2 in Table 6.6 and Figure 6.11 show that the optimum purge angle in this case is greater than 0.20. At $\beta_{11} = 0.20$, the dehumidification per unit process stream flow, η_{wp} , is about 25% greater than at $\beta_{11} = 0.0$, which is a greater improvement than was observed for the low thermal capacitance dehumidifier. Again, a maximum in η_{wp}^* , the dehumidification per unit total period flow, is obtained for inlet state 2 at $\beta_{11} \approx 0.10$. The dehumidification has increased by about 8%, nearly double the improvement obtained for the low capacitance dehumidifier with inlet state pair 2. However, as was the case for inlet state pair 1, the low thermal capacitance dehumidifier has low process stream outlet humidity ratios than the high thermal capacitance dehumidifier.

The solutions for inlet state pair 2 indicate that the recirculated purge can improve the dehumidification per unit period flow, η_{wp}^* , by 4% for the low thermal capacitance matrix and by 8%

for the high thermal capacitance matrix. The enhanced effect of purging for inlet state pair 2 compared to inlet state pair 1 is due to the much greater difference between regenerating inlet and the process outlet humidity ratios for inlet state pair 2. Whether these improvements in dehumidifier performance are significant depends on the constraints imposed on the dehumidifier design and operating conditions. For example, suppose that the inlet states are fixed at state pair 2, and the dehumidifier performance can only be modified by changing the flow length Λ_{jk} . Numerical results indicate that for both the low and high thermal capacitance matrices Λ_{jk} must be increased to more than 80 in order for an unpurged ($\beta_{11} = 0$) dehumidifier to have the same dehumidification per unit period flow as the optimum purged dehumidifier with $\Lambda_{jk} = 20$, which is a substantial change in dehumidifier geometry. Alternatively, suppose that the dehumidifier dimensions and flow rates are fixed, but that the regenerating temperature of inlet state pair 2 may be varied. Numerical results show that the regeneration temperature of the unpurged low thermal capacitance dehumidifier must be boosted from 85°C to 88.5°C in order to give the same performance as the optimum purged dehumidifier with an 85°C regeneration temperature. Similarly, the regeneration temperature of the unpurged high thermal capacitance dehumidifier must be increased from 85°C to 89.5°C. The unpurged dehumidifier requires a greater input of thermal energy to the regenerating stream to match purged dehumidifier performance not only because the required regeneration

temperatures are higher but because the regenerating flow rate is greater than in the purged dehumidifier by a factor of $(1 - \beta_{11})^{-1}$. Thus, for inlet state pair 2, the energy requirement for an unpurged low capacitance dehumidifier is at least 6% greater than that of the optimum purged dehumidifier, while the unpurged high capacitance dehumidifier requires over 10% more energy input than the equivalent purged dehumidifier.

6.4 Design Point Performance of Desiccant Cooling Systems with a Purged Dehumidifier

The dehumidifier inlet states in a ventilation and recirculation cycle desiccant cooling system operating at SERI standard design conditions [105] are inlet state pairs 1 and 2 respectively. The data presented in the preceding section can be used to demonstrate the effect on the design point performance of these systems of incorporating a purged dehumidifier.

The cooling system performance is expressed in terms of the specific cooling capacity and the thermal COP, as in §4.5. In this case, the specific cooling capacity can be defined on the basis either of the air flow delivered to the cooling load or of the total air flow through period 1 of the dehumidifier (process plus purged flow rates). The process stream specific cooling capacity is greater than the cooling capacity per unit total period 1 flow by a factor of $1/(1 - \beta_{11})$, just as $\eta_{wp} = \eta_{wp}^*/(1 - \beta_{11})$.

The COP is the same in either case.

The ventilation and recirculation system performance will be determined only for the 12 purge geometry, since this purge geometry results in slightly lower dehumidifier process stream outlet humidity ratios than that obtained with the 11 purge configuration. As in §4.5, the heat exchanger carryover is neglected and the effectiveness is 0.95, and the evaporative coolers are assumed to saturate the air streams.

The variation of the design point performance of the ventilation cycle air conditioner with purge angle β_{11} is shown in Figure 6.12 for both the low and high thermal capacitance dehumidifiers. Comparison of the results for the two systems show that the specific cooling capacity of the high thermal capacitance dehumidifier system is about 20% less than that of the system with the low thermal capacitance dehumidifier, but the two systems have nearly equal thermal COP. In both systems, the process stream cooling capacity increases with increasing purge angle, reflecting the corresponding decrease in the dehumidifier process stream humidity ratio. The system with a low thermal capacitance dehumidifier has a maximum in process stream specific capacity at about $\beta_{11} = 0.10$ that is about 10% greater than the specific capacity for the unpurged system. The corresponding maximum for the system with a high thermal capacitance dehumidifier is at $\beta_{11} = 0.20$, and is about 15% greater than obtained with $\beta_{11} = 0.0$. In both systems, the cooling capacity per unit total period flow is nearly constant for